The DOI for this manuscript is doi: 10.1175/2009JPO4213.1

Upper Ocean Processes Under the Stratus Cloud Deck in the Southeast Pacific Ocean.

Yangxing Zheng[1], Toshiaki Shinoda[2], George N. Kiladis[1], Jialin Lin[3], E. Joseph Metzger[2], Harley E. Hurlburt[2], and Benjamin S. Giese[4]

[1]NOAA ESRL/CIRES Climate Diagnostics Center, Boulder, Colorado

[2]Naval Research Laboratory, Stennis Space Center, Mississippi

[3]Department of Geography, The Ohio State University, Columbus, Ohio

[4]Department of Oceanography, Texas A&M University, College Station, Texas

Journal of Physical Oceanography

January 2009 (submitted)

June 2009 (revised)

July 2009 (revised)

Corresponding author address:

Yangxing Zheng

NOAA ESRL/CIRES Climate Diagnostics Center, 325 Broadway, R/PSD1, Boulder, Colorado, 80305

Yangxing.Zheng@noaa.gov

Tel: (303) 497-4592

ABSTRACT

The annual mean heat budget of the upper ocean beneath the stratocumulus/stratus cloud deck in the southeast Pacific is estimated using Simple Ocean Data Assimilation (SODA) and an eddy-resolving HYbrid Coordinate Ocean Model (HYCOM). Both are compared with estimates based on WHOI IMET buoy observations at 85^{o}W, 20^{o}S. Net surface heat fluxes are positive (warming) over most of the area under the stratus cloud deck. Upper ocean processes responsible for balancing the surface heat flux are examined by estimating each term in the heat equation. In contrast to surface heat fluxes, geostrophic transport in the upper 50 m causes net cooling in most of the stratus cloud deck region. Ekman transport provides net warming north of the IMET site and net cooling south of the IMET site. Although the eddy heat flux divergence term can be comparable to other terms at a particular location such as the IMET mooring site, it is negligible for the entire stratus region when area averaged, since it is not spatially coherent in the open ocean. While cold core eddies are often generated near the coast in the eddy-resolving model, they do not significantly impact the heat budget in the open ocean in the southeast Pacific.

1. Introduction

Sea surface temperature (SST) in the southeast Pacific near the coasts of Peru and Chile is colder than at any comparable latitude elsewhere. It is believed that these cold waters in the southeast Pacific play an important role in the formation and maintenance of persistent stratocumulus/stratus cloud decks, and that these clouds have a significant impact on regional and global climate (e.g., Ma et al. 1996; Miller 1997; Gordon et al. 2000; Xie 2004). Thus, it is important to understand upper ocean processes that maintain SST under the stratocumulus cloud deck for global simulation and climate prediction. However, until recently, the upper ocean in this region has been sparsely observed, which limits our ability to better understand and simulate the behavior of the atmosphere and ocean globally. In fact, most coupled atmosphere-ocean general circulation models (CGCMs) have systematic errors in the southeast Pacific, including too warm SSTs and too little cloud cover (e.g., Mechoso et al. 1995; Ma et al. 1996; Lin 2007), which have important impacts on the simulated radiation budget and climate sensitivity.

As part of the Eastern Pacific Investigation of Climate (EPIC), a well-instrumented surface mooring was deployed under the middle of the stratus cloud deck (85^{o}W, 20^{o}S) in October 2000, providing 6 years of upper ocean temperature, salinity, velocity, and surface meteorological variables (Colbo and Weller 2007). Using these data sets as well as other satellite and historical data, Colbo and Weller (2007) estimated the upper ocean heat budget (upper 250 m) at the location of the mooring in order to understand upper ocean processes that maintain the annual mean heat content of the upper ocean in this region. They found that the major terms of the heat equation that balance positive (warming) surface heat fluxes are geostrophic heat transport and eddy heat flux divergence. Based on the results of their analysis, they hypothesized that cooling due to the eddy heat flux divergence is a result of westward propagation of cold coherent eddies formed near the coast that slowly decay in the open ocean.

While the analysis of Colbo and Weller (2007) at the IMET site significantly improved our understanding of the upper ocean in this region, a variety of assumptions were made in their estimates since it is difficult to calculate all terms in the heat equation from the data at one location. In particular, the eddy heat flux divergence was estimated as a residual from the closure of the heat budget in the heat equation. Also, while the estimates for the upper 250 m layer help understand processes that control the upper ocean heat content, SSTs may not be directly affected by advection and eddy fluxes around 250 m depth since the deepest mixed layer depth during winter is ~150 m. Furthermore, the persistent stratus cloud decks occupy a large portion of southeast Pacific (Klein and Hartmann 1993; Colbo and Weller 2007), and it is difficult to identify important upper ocean processes for the entire stratus region from an analysis of one location.

In this study, three-dimensional upper ocean processes for the entire stratus cloud region are examined using Simple Ocean Data Assimilation (SODA; Carton and Giese 2008) and an eddy-resolving ocean general circulation model (OGCM), i.e., the HYbrid Coordinate Ocean Model (HYCOM). The data sets obtained from the mooring observations are utilized to evaluate the model performance. The annual mean of the terms contributing to the heat budget are calculated at the mooring site and compared with observational estimates. Contributing terms are also estimated for the entire stratus cloud deck region in order to examine the representativeness of the mooring site for broad scale upper ocean processes. In addition, terms contributing to the heat budget in the upper 50 m are computed from the model output in order to improve our understanding of upper ocean processes that control sea surface temperature variability in this region. In particular, the relative importance of horizontal heat advection and eddy heat flux divergence in the upper ocean heat budget is emphasized and the role of cold core eddies generated near the coast in the open ocean heat budget is also discussed.

2. Models and data sets

2.1 SODA

The SODA methodology, the ingested data, and the error covariance structure of both the model and the observations are described by Carton et al. (2000a, b), Carton and Giese (2008), and Zheng and Giese (2009). The ocean model is based on the Los Alamos implementation of the Parallel Ocean Program (POP) (Smith et al. 1992). The model resolution is on average 0.4^{o} (lon) X 0.25^{o} (lat) with 40 levels in the vertical. The model is forced with the European Centre for Medium-Range Weather Forecasts (ECMWF) ERA-40 daily atmospheric reanalysis winds (Simmons and Gibson 2002) for the 44-year period from 1958 to 2001. We update the analysis in a second run forced by QuikSCAT wind stress from 2002 to 2005.

Surface heat fluxes are computed from bulk formulae (Smith et al. 1992), with atmospheric variables that come from the NCEP/NCAR reanalysis (Kalnay et al. 1996). The NCEP/NCAR reanalysis information is used for the bulk formulae instead of the ERA-40 variables throughout the experiment to give continuity of surface forcing during periods for which the ERA-40 winds are not available. However, the details of surface heat flux boundary condition are relatively unimportant in influencing the solution, since near-surface temperature observations are used to update the mixed layer temperature. Vertical diffusion of momentum, heat, and salt is based on a non-local K-Profile parameterization (KPP, Large et al. 1994) scheme and horizontal diffusion for subgrid-scale processes is based on a biharmonic mixing scheme.

The model is constrained by observed temperature and salinity using a sequential assimilation algorithm, which is described by Carton et al. (2000a, b) and Carton and Giese (2008). The basic subsurface temperature and salinity observation sets consist of approximately 7×10^6 profiles, of which two-thirds have been obtained from the World Ocean Database 2001 (Boyer et al. 2002; Stephens et al. 2002) with online updates through December 2004. This dataset has been extended by the addition of real-time temperature profile observations from the Tropical Atmosphere-Ocean/Triangle Trans-Ocean Buoy Network (TAO/TRITON) mooring thermistor array and Argo floats. In addition to the temperature profile data, a large number of near-surface temperature observations are available both in the form of *in situ* observations [bucket and ship-intake temperatures from the Comprehensive Ocean-Atmosphere Data Set (COADS) surface marine observation set of Diaz et al. 2002] and from satellite remote sensing. SODA used the nighttime NOAA/National Aeronautics and Space Administration (NASA) Advanced Very High Resolution Radiometer (AVHRR) operational SST data, which began November 1981 and average 25000 samples per week. Use of only nighttime retrievals reduces the error due to skin temperature effects. However, the biggest challenge in retrieving SST from an IR instrument in the southeast Pacific Ocean is the cloud detection problem since clouds are opaque to infrared radiation and can effectively mask radiation from the ocean surface. Carton et al. (2000a,b) used a bias-corrected model error covariance in an attempt to reduce such error. The near-surface salinity observation set averages more than 10^5 observations per year since 1960 (Bingham et al. 2002). Nearly continuous sea level information is available from a succession of altimeter satellites beginning in 1991. Although the coverage of subsurface data in the southeast Pacific Ocean is not as good as other regions in the tropics, a significant amount of satellite observations are used in SODA especially after 1980 (not shown). The yearly number of observations in the southeast Pacific (140^{o}W-70^{o}W, 35^{o}S-5^{o}S) exceeds 10^5 after 1984. Hence it is likely that SODA analysis can provide more accurate estimates of mean heat advection than models with no data assimilation.

Averages of model output variables (temperature, salinity, and velocity) are saved at 5-day intervals. These average fields are remapped onto a uniform global 0.5^o X 0.5^o horizontal grid using the *horizontal grid spherical coordinate remapping and interpolation package* with second-order conservative remapping (Jones 1999).

2.2 HYCOM

HYCOM was developed from the Miami Isopycnic Coordinate Ocean Model using the theoretical foundation set forth in Bleck and Boudra (1981), Bleck and Benjamin (1993), and Bleck (2002). A description of the recent version of global HYCOM used in this study can be found in Hurlburt et al. (2008). HYCOM uses a generalized vertical coordinate that is normally isopycnal in the open stratified ocean, but which makes a dynamically smooth transition to pressure coordinates (nearly z-level) in the mixed layer and other unstratified or weakly stratified water, and to σ (terrain-following) coordinates in shallow water, although it is not limited to these coordinate choices. Another key feature of HYCOM is that it can have zero thickness layers, allowing isopycnals to intersect sloping topography. Where HYCOM uses pressure coordinates, partial cell topography is an automatic consequence of the generalized vertical coordinate design. The system is configured for the global ocean with HYCOM 2.2 as the dynamical model. Computations are carried out on a Mercator grid between 78^{o}S and 47^{o}N with a horizontal resolution of 1/12^o X 1/12^o cos(latitude). North of 47^{o}N the global model grid is a bipolar cap with the singularities placed over Asia and North America. There are 32 layers in the vertical. Bottom topography is derived from a quality controlled NRL DBDB2 (Naval Research Laboratory Digital Bathymetry Data Base with 2-minute resolution) dataset. Three-hourly surface forcing is from the Navy Operational Global Atmospheric Prediction System (NOGAPS) (Rosmond et al. 2002) and includes wind stress, wind speed, heat flux (using bulk formula) (Kara et al. 2005c), and precipitation.

HYCOM uses a penetrating solar radiation scheme that accounts for the effects of spatial and temporal variations in water turbidity (Kara et al. 2005a). This scheme is designed to improve the simulation of upper ocean quantities, especially SST. The net longwave flux is the sum of downward longwave (from the atmosphere) and upward blackbody radiation. The blackbody radiation from ERA-40 is corrected to allow for the difference between ERA-40 SST and HYCOM SST (Kara et al. 2005b). Latent and sensible heat fluxes at the air-sea interface are computed using efficient and accurate bulk parameterizations (Kara et al. 2005c).

As in SODA, KPP is used for vertical mixing in the model. Global HYCOM was integrated for the time period from January 2003 to April 2007. During this period, the tropical Pacific Ocean was in a near-normal condition with no strong El Nino and La Nina events. In this study, model output from HYCOM is used primarily for identifying the role of eddies in the heat budget of the upper ocean under the stratus cloud deck in the southeast Pacific.

2.3 Data sets

The data set used in this study is from a well-instrumented IMET buoy developed at the Woods Hole Oceanographic Institution (WHOI) and deployed at 85^{o}W, 20^{o}S in October 2000. Six years of high quality data (8 October 2000 to 18 October 2006) were used here. The surface heat fluxes are calculated using SST and surface meteorological variables from the IMET buoy using the Tropical Ocean Global Atmosphere-Coupled Ocean Atmosphere Response Experiment (TOGA- COARE) bulk air-sea flux algorithm version 2.6 (Bradley et al. 2000). More detailed description of IMET data sets can be found in Colbo and Weller (2007). The World Ocean Atlas 2005 (WOA05) monthly temperature and salinity climatology is also used for determining uncertainties in the model's annual mean horizontal heat advection. The gridded ($1/3^{o}$ X $1/3^{o}$, Mercator grid) product of Topex/Poseidon, ERS-1/2, and Jason-1/Jason-2 sea surface heights and geostrophic currents (computed from absolute topography) produced by Ssalto/Duacs and distributed by Archiving Validation and Interpretation of Satellite Data in Oceanography (AVISO) are used to validate the model's ability to simulate eddy activity. The data set spans 22 August 2001 – 28 February 2009.

3. Comparisons with the IMET observations

We first compare the surface heat flux used to force HYCOM and subsurface temperature in SODA and HYCOM with those from the IMET buoy observations at 20°S, 85°W. Note that surface heat fluxes used for SODA are not available.

3.1 Surface heat flux

Figure 1 shows the time series of the 5-day averaged net surface heat flux estimates at (85°W, 20°S) for HYCOM and the IMET observations spanning 3 January 2004 – 8 December 2004. The net surface heat flux is computed based on the shortwave radiation, longwave radiation, surface sensible and latent heat fluxes from NOGAPS atmospheric variables and HYCOM's SST. The seasonal variation of surface heat flux based on NOGAPS agrees with the IMET estimate reasonably well (correlation coefficient = 0.78). However, there are significant differences between estimates based on the IMET and NOGAPS. For example, during January - early February, and September - November, IMET estimates are larger by ~80 W m^{-2}. The root-mean-square (RMS) difference is 53 W m^{-2} using the 5-day means over this period. Because of these discrepancies, the mean surface heat flux from IMET observations is significantly larger (Table 1). Nevertheless, as will be discussed in section 3.3, the net surface heat fluxes based on NOGAPS are positive (warming) in most areas discussed in this study, which is consistent with the IMET estimate. In order to further confirm the spatial distribution of surface heat flux in this region, we have examined the annual mean heat fluxes in the Objectively Analyzed Air-sea Fluxes (OAFlux, Yu and Weller 2007; Yu et al. 2008) and other atmospheric reanalyses (NCEP1, NCEP2, ERA-40). All data sets show the net surface heat fluxes are positive in most of the stratus region (not shown). Hence the surface heat flux estimates based on NOGAPS are suitable for driving the HYCOM in this study, which primarily examines upper ocean processes that balance the positive surface heat fluxes in the stratus region.

3.2 Upper ocean temperature

Model simulations of tropical oceans using HYCOM were previously evaluated by comparing with *in situ* and satellite observations (Shaji et al. 2005; Han 2005; Han et al. 2006; Shinoda et al. 2008; Shinoda and Lin 2009). These studies show HYCOM is able to simulate upper ocean variability reasonably well, including that within the stratus cloud deck region.

Figure 2 shows the temperature evolution in the upper 300 m from IMET observations, and from the nearest grid points in SODA and HYCOM over 1 October 2004 – 31 October 2005. Both SODA and HYCOM are able to capture the seasonal evolution of the mixed layer, in which the mixed layer depth is about 20-30 m in the Austral summer (February-March) and becomes deepest (~150 m) after the Austral winter (September-October). The thermocline structure is better reproduced in SODA than HYCOM. This is because observational data were not assimilated into the HYCOM simulation. Nevertheless, given the fact that seasonal evolution of the mixed layer (above ~150 m) is well reproduced by models, these experiments are suitable for this study, which primarily discusses estimates of the heat budget in the upper 50 m. It should be noted that the agreement between models and observations in other years is similar to this period (not shown).

3.3 Mean heat budget

The heat equation integrated over several years and down to some depth z_0, is

$$\int_0^{years}\int_{z_0}^{0}\frac{\partial T}{\partial t}dzdt=\int_0^{years}\left(\frac{Q_{net}}{C_p\rho}-\int_{z_0}^{0}\left(\mathbf{V}\bullet\nabla_h T+w\frac{\partial T}{\partial z}+\nabla\bullet\left(\overline{\mathbf{V}'T'}\right)+\kappa_h\nabla^2 T\right)dz-\kappa_v\frac{dT}{dz}\Big|_{z_0}\right)dt$$

where Q_{net} is the net surface heat flux, C_p is the specific heat of sea water at constant pressure, ρ is the density of sea water, w is the vertical velocity, $\mathbf{V}$ is horizontal velocity vector, T is temperature, $\mathbf{V}'$ and T' are deviations from the seasonal mean. z_o is assumed to be deep enough so that the penetrative component of shortwave radiation is within the layer. $\nabla\bullet\left(\overline{\mathbf{V}'T'}\right)$ on the right-hand side is the divergence of eddy heat flux. The time scale of the mean has to be defined to calculate this term. Following some previous studies (Penven et al. 2005; Colbo and Weller 2007), we use the seasonally averaged velocity and temperature (~ 90-day averages) as the mean values in this study. Accordingly, $\mathbf{V}$, w, and T are the seasonally averaged values from 5-day averaged data. The first term on the left-hand side is the rate of temperature change (or temperature tendency), which is negligible when averaged over several years. The terms on the right-hand side are net surface heat flux, horizontal heat advection, vertical heat advection, divergence of eddy heat flux, and horizontal and vertical diffusion, respectively. In this study, horizontal advection and the divergence of eddy heat flux are the primary focus of the discussion. Colbo and Weller (2007) suggest that these terms are important and they can be reliably estimated from the model output. Note that some of the other terms are difficult to estimate from the model output because of variable unavailability and the errors due to coordinate transformation and interpolations.

Table 1 shows the mean heat flux due to geostrophic and Ekman currents, and eddy heat flux divergence in the upper 250 m at 85^{o}W, 20^{o}S from the models and Colbo and Weller's (2007) estimates based on IMET datasets. The numbers of Colbo and Weller's estimates in this table are obtained directly from their paper (Colbo and Weller 2007). The periods for the averaging are October 2000 to December 2004 for Colbo and Weller's (2007) estimates, January 1980 to November 2005 for SODA, and January 2003 to April 2007 for HYCOM. We note that the eddy flux divergence was computed as a residual in Colbo and Weller (2007). Geostrophic currents are computed from the model temperature and salinity. Ekman currents are calculated from the difference between geostrophic and total velocities. This approximation will be discussed in Section 4.3. While it is unlikely that quantitative agreement of these estimates would be found at one location because of the variety of assumptions made for the observational estimates, model deficiencies, and the errors in the surface forcing fields, it is noteworthy that some of the terms estimated from the models are reasonably consistent with the Colbo and Weller's estimates. For instance, the cold advection due to geostrophic transport in SODA and HYCOM is comparable to their estimates. Heat advection due to Ekman transport in SODA is also consistent with their estimates. Eddy flux divergence is large at the IMET site in the Colbo and Weller's estimates as well as in the models, though HYCOM gives a positive sign. The difference in geostrophic heat transport is mostly due to the zonal component of geostrophic currents and the meridional temperature gradient (not shown).

In order to examine the representativeness of the mooring observations at a particular location for broad scale upper ocean variability in this region, we calculated the mean heat budget (0-250 m) in SODA and HYCOM averaged over the region (100^oW-80^oW, 30^oS-10^oS) where the largest annual mean low cloud cover is found (Colbo and Weller 2007) (Table 2). We keep tenths of a unit for those estimates whose values are between -1 and +1 W m^{-2} in order to identify the sign. The results are consistent between the two models. First, cooling from geostrophic transport is large both SODA and HYCOM. Second, warm advection due to Ekman transport is small, especially in SODA. Finally, the eddy heat flux divergence term is significantly small in both models and is negligible over this region. We have also examined the average over a few different boxes and find that the main conclusions are similar to those averaged in the box (100^oW-80^oW, 30^oS-10^oS) presented here.

We also computed these terms at 85^oW, 20^oS in the upper 50 m (Table 3) since horizontal heat advection and eddy heat flux divergence around 250 m may not directly affect SST, especially when the mixed layer is shallow. Heat advection due to Ekman transport at the IMET site is not much smaller than that due to geostrophic transport, since the Ekman currents are confined to the upper shallow layers. Eddy heat flux divergence provides a small cooling in SODA and a warming in HYCOM. If averaged over the entire stratus cloud deck region (100^oW-80^oW, 30^oS-10^oS) (Table 4), Ekman heat advection in SODA is smaller than geostrophic heat advection. In addition, the area averaged eddy heat flux divergence becomes negligible for both SODA and HYCOM. The role of eddies in the upper ocean heat budget will be discussed further in Section 4.5.

4. Spatial distribution of the upper ocean heat budget

In this section, the spatial distribution of major contributing terms, discussed in the previous section, is examined. We explore how geostrophic and Ekman transports and the divergence of eddy flux contribute to the upper ocean heat budget by analyzing the model output in the entire stratus cloud deck region.

4.1 Net surface heat flux

The net surface heat flux computed from NOGAPS and HYCOM's SST was averaged over the period 2003-2007 (Figure 3). It is positive (warming the ocean) over most of the region, including the IMET site (marked by an "X" on the map). Strong warming from the net surface heat flux is found near the coast south of 15^{o}S. This warming must be balanced by other processes, such as Ekman currents and strong coastal upwelling there. Over the open ocean beneath the stratus cloud deck, the warming due to the net surface heat flux is weaker.

We also examined the net surface heat flux in the OAFlux (Yu and Weller 2007; Yu et al. 2008) and other atmospheric reanalyses (NCEP1, NCEP2, ERA-40) to confirm that the spatial pattern is similar in other datasets (not shown). Net surface fluxes from all data sets show positive (warming of the ocean) in most of the stratus region, although there are some quantitative differences. This suggests that the surface heat fluxes used to force the model are appropriate for this particular study, which examines upper ocean processes responsible for balancing the positive surface heat fluxes.

4.2 Geostrophic heat advection

Horizontal heat advection due to geostrophic currents was computed from the SODA and HYCOM output. Geostrophic currents are computed with respect to the ocean hydrography (i.e., the model temperature and salinity). Figure 4 shows temporal mean geostrophic heat advection and geostrophic currents and temperatures in the upper 50 m from SODA and HYCOM. The periods for the averaging are 1980-2005 for SODA, and 2003-2007 for HYCOM. It should be noted that we have also calculated the spatial distribution of this term as well as other terms in the heat equation using a period (2003-2005) that both SODA and HYCOM cover, and found that the results are similar.

In contrast to warming over most of the stratus cloud deck region from net surface heat flux, geostrophic transport causes significant upper ocean cooling over most of the stratus cloud deck region. The way in which geostrophic currents produce cooling is demonstrated by the map of temperature and geostrophic currents in SODA and HYCOM (Figures 4c, 4d). Northwestward geostrophic currents in most of the stratus region cross the isotherms that are nearly perpendicular to the direction of the currents, and thus geostrophic currents transport cold water to the stratus cloud region. In some locations, for example, in the region south of 30^{o}S between 100^{o}W-90^{o}W, geostrophic currents flow along the isotherms and thus the heat transport due to geostrophic currents is negligible compared to that due to Ekman currents. However, overall in the region shown in Figure 4, our analysis indicates that geostrophic transport plays an important role in the upper ocean heat budget, which is consistent with Colbo and Weller's estimates using the IMET datasets (2007).

In order to examine the uncertainty of annual mean geostrophic advective heat flux from SODA and HYCOM, we have also calculated this term using WOA05 temperature and salinity climatology (not shown). The magnitude and spatial pattern of this term based on the data agree with those from the models reasonably well. Geostrophic currents calculated from WOA05 data provide cooling most of the stratus cloud region. RMS difference with respect to the WOA05 data in the entire stratus cloud region (100^{o}W-80^{o}W, 30^{o}S-10^{o}S) is 5.7 W m^{-2} for SODA and 11.1 W m^{-2} for HYCOM.

4.3 Ekman transport of heat

Figure 5 shows the temporal mean Ekman heat transport and the temperature and Ekman currents from SODA and HYCOM in the upper 50 m. In SODA, the Ekman transport causes warming north of the IMET site and cooling south of the IMET site. Because the IMET site (85^{o}W, 20^{o}S) is located near the boundary between positive and negative heat advection, the magnitude of Ekman heat advection is minimal around this site. The overall spatial distribution of heat transport and the relation between currents and temperature in HYCOM are similar to those in SODA. However, there are more fine scale structures in HYCOM in the region south of 16^{o}S. It is unlikely that these fine structures are caused by the currents directly driven by local winds. In this study, however, we still retain the term "Ekman" while acknowledging these fine scale features may not be the results of heat transport caused by currents directly generated by local winds.

In order to examine the uncertainty of Ekman advective heat flux from models, we have also computed Ekman heat transport from the WOA05 temperature climatology and ERA-40 wind stress climatology (not shown). The spatial pattern of Ekman advective heat flux calculated from the data is very similar to that from the models, indicating that the large scale features of this term are well captured by the models. RMS difference of annual mean values with respect to the WOA05 data in the stratus cloud region (100°W-80°W, 30°S-10°S) is 8.8 W m^{-2} for SODA and 11.7 W m^{-2} for HYCOM.

In order to examine whether the difference between total and geostrophic currents is a good approximation of Ekman currents, we also calculated Ekman transport directly using ERA-40 wind stress (1980-2001) and QuikSCAT wind stress (2002-2005) using the equation:

$$M_x = \frac{\tau_y}{\rho f}$$

$$M_y = -\frac{\tau_x}{\rho f},$$

as well as the Ekman advective heat flux with the equation:

$$H_{ek} = H_x + H_y = \frac{C_p \tau_y}{f}\frac{dT_{mld}}{dx} + \left(-\frac{C_p \tau_x}{f}\frac{dT_{mld}}{dy}\right)$$

where M_x, M_y are zonal and meridional Ekman transports, H_x, H_y are zonal and meridional Ekman advective heat flux, (τ_x, τ_y) are zonal and meridional wind stress from SODA, T_{mld} is mixed layer temperature in SODA, ρ is sea water density, $f = 2\Omega \sin\theta$ is the Coriolis parameter, and C_p is the specific heat capacity at constant pressure. The resulting Ekman transport and Ekman advective heat flux in the mixed layer averaged over 1980-2005 are shown in Figure 6. Figure 6 also displays mixed layer temperature from SODA. Ekman advective heat flux in Figure 6 is quite similar to that in Figure 5a. Ekman transport causes net warming north of the IMET site and net cooling south of the IMET site. This provides justification for calculating Ekman heat advection using ageostrophic currents from the model output. The Ekman transport is nearly parallel to the mean SST isotherms in the offshore region near the IMET site, which is consistent with the result from Colbo and Weller (2007), although they used different data sets and a different analysis period.

4.4 Vertical heat advection

Figure 7a shows the vertical heat advection in the upper 50 m calculated from SODA. It is evident that vertical advection causes weak warming in the open ocean but not in the coastal region where strong upwelling occurs. The cooling due to the upwelling near the coast is balanced by the positive net surface heat flux (Figure 3). Figure 7b shows the velocity and temperature section along 20^{o}S. A pronounced vertical circulation centered around 40m deep is evident at 78^{o}W. Cold water upwelled near the coast is transported offshore by mean flow in the upper 40 m. Because of the downwelling caused by the convergence of surface currents in the open ocean, the weak subsurface warming occurs due to the vertical heat advection in broad areas of the stratus region.

It should be noted that the vertical heat advection in z coordinates is non-trivial to calculate reliably from the available HYCOM output. This is because HYCOM's natural coordinate system uses time dependent hybrid layers rather than fixed z-levels, and interpolated vertical velocities in z-coordinates derived from the derivative of horizontal velocity at each level (layer) contain large errors.

4.5 Eddy heat flux divergence

In this section, heat transport caused by eddies in models are discussed. We first compare eddy fields in models with those in satellite observations in order to examine whether models are able to generate realistic eddies in this region. Then eddy heat flux divergence is computed in the entire stratus cloud region to identify the role of eddies in overall heat balance in this region.

a. Eddy kinetic energy

Eddy activity in models is examined by calculating eddy kinetic energy (EKE). In order to demonstrate how well the models can generate realistic eddies, we compare EKE from models with that derived from satellite altimeters (i.e, AVISO surface geostrophic velocity). HYCOM's surface geostrophic velocity is first averaged onto a 1/3^o X 1/3^o grid in order to match the spatial resolution of AVISO geostrophic velocity. Then EKE is computed as EKE = $\left(u'^{2}_{geo} + v'^{2}_{geo}\right)/2$), where u'_{geo} and v'_{geo} are deviations of the 5-day averaged geostrophic velocity from its seasonally averaged values. Data on a 0.5^o X 0.5^o grid are used for SODA. Figure 8 shows the map of annual mean surface EKE (in cm^2 s^{-2}) from SODA, HYCOM, and AVISO. The magnitude and spatial pattern of EKE in HYCOM are similar to those from observations. In HYCOM and observations, eddies are more active near the coastal region than in the open ocean (Figures 8b, 8c). Since HYCOM uses sufficiently fine horizontal resolution to resolve mesoscale eddies, its overall eddy activity is much higher than that in SODA, which uses a relatively coarse resolution. Despite the general agreement between HYCOM and observations, there are some notable differences. For example, EKE in HYCOM is larger than observations near the coast. In the open ocean, particularly in the region of 20^{o}S-15^{o}S, 100^{o}W-90^{o}W, the EKE is higher than observations.

Eddy activity in the southeast Pacific Ocean has been also reported in some previous studies (Hormazabal et al. 2004; Chaigneau and Pizarro 2005a,b; Penven et al. 2005). The spatial distribution and magnitude of mean EKE in HYCOM shown in Figure 8 are similar to those derived from drifter data (Chaigneau and Pizarro 2005a) and satellite altimeter data (Hormazabal et al. 2004; Penven et al. 2005). The good agreement of eddy fields between HYCOM and observations suggests that the HYCOM output is suitable for examining the role of eddies in the upper ocean heat budget in this region.

The enhanced eddy activity along the coast can be explained by many processes. For instance, the interaction of the Peru-Chile Current system with the coastline is able to produce the active eddies (Chaigneau and Pizarro 2005a). Coastal flows with large interannual and seasonal variability are relevant to disturbances of equatorial origin that may reinforce the unstable coastal jet (Pizarro et al. 2002; Zamudio et al. 2006, 2007). Also the strong upwelling fronts observed in spring and summer could generate baroclinic instabilities that may enhance mesoscale variability. Furthermore, downwelling coastal Kelvin waves can strongly intensify the Peru-Chile Undercurrent system (Shaffer et al. 1997), which may destabilize the near surface coastal circulation generating eddies.

It should be noted that EKE in AVISO data is computed from the deviation of surface geostrophic velocity, which could be much weaker than the total velocity deviation. We also calculated the EKE using total velocities from SODA and HYCOM (i.e., EKE = $\left(u'^2 + v'^2\right)/2$), where u' and v' are deviations of the total velocity from their seasonally averaged values. Figure 9 illustrates the annual mean of EKE derived from the total velocity. The EKE values in SODA and HYCOM are significantly higher in both the open ocean and near the coast than those derived from geostrophic velocity. This suggests that the eddy kinetic energy calculated from AVISO data can be underestimated since only a geostrophic component of velocity field is used.

b. Eddy characteristics

In order to further illustrate the characteristics of eddies simulated in HYCOM, the vertical component of vorticity and the Okubo-Weiss parameter (OWP) at 30 m depth were computed. Figures 10a and 10d show HYCOM temperatures (in ^{o}C) and currents (in m s^{-1}) at 30 m depth in the southeast Pacific Ocean associated with the mesoscale ocean eddy field on January 8 2004 and June 21 2004. OWP on these dates are also shown in Figure 10c and 10f. The OWP is defined as:

$$OWP = \left(\frac{\partial u}{\partial x} - \frac{\partial v}{\partial y}\right)^2 + \left(\frac{\partial v}{\partial x} + \frac{\partial u}{\partial y}\right)^2 - \left(\frac{\partial v}{\partial x} - \frac{\partial u}{\partial y}\right)^2$$

where u and v are the horizontal velocity components, and x and y are the horizontal coordinates. The first two terms on the right hand side represent the deformation and the last term is the vertical component of the relative vorticity. If OWP is positive (negative), the deformation (relative vorticity) dominates. Therefore the OWP helps identify the boundary of eddies since eddies are generally characterized by a strong rotation in their center, and a strong deformation in their periphery. Thus eddies can be demonstrated by patches of negative values of OWP surrounded by positive rings. The snapshot of subsurface vorticity (Figures 10b, 10e) indicates a succession of cyclones and anti-cyclones, which is generated at the upwelling front. Eddies are clearly seen in the image of the OWP (Figures 10c, 10f). They appear more energetic near the coastal area. In the open ocean including near the IMET site, the eddies clearly exist, although they are relatively weaker. These spatial distributions are consistent with the spatial pattern of the EKE.

c. Example of cold core eddies

Colbo and Weller (2007) speculated that the cooling at the IMET site due to eddy heat flux divergence is likely to be caused by the cold core eddies that have been advected offshore from the upwelling region where these eddies are generated. In order to identify such cold eddies in HYCOM, temperature and velocity anomalies during the entire period of the experiment are inspected.

Figure 11 shows the maps of temperature and velocity anomalies averaged in the upper 50 m during March 2005. The anomalies of temperature and velocity are derived from the 2003-2007 pentad climatology. Many anti-cyclonic/cyclonic eddies associated with warm/cold waters are found near the coast. During this period, an eddy associated with cold waters and cyclonic circulation around 20^{o}S, 74^{o}W on March 8 propagates westward and reaches around 76^{o}W on March 28. Similar westward propagating cold core cyclonic eddies are frequently found in HYCOM. However, these cyclonic eddies associated with cold waters in the upper layer are mostly found within several degrees away from the coastline, and seldom propagate to locations near the IMET site during the period of model experiment.

d. Roles of eddy heat flux

The eddy heat flux divergence is computed following the definition $-\left(\partial u'T'/\partial x + \partial v'T'/\partial y\right)$, where u', v' and T' are deviations of the total velocity and temperature (5-day averaged) from their seasonally averaged values. Figure 12 shows the spatial distribution of mean eddy heat flux divergence in the upper 50 m from SODA and HYCOM. Because of the weak eddy activity in SODA, the eddy flux divergence is very small in the entire stratus region. The magnitude of eddy flux divergence in HYCOM is much larger than that in SODA, particularly near the coast. Near the IMET site, the temporal mean of eddy heat flux in HYCOM is positive (+6 W m^{-2}), which could be significant at this location. However, unlike geostrophic and Ekman heat transports, the eddy flux divergence term is not spatially coherent. As a result, the temporal mean of eddy heat flux averaged over 30^{o}S-10^{o}S, 100^{o}W-80^{o}W is much smaller (see Table 2, Table 4) than the estimate by Colbo and Weller (2007) at the IMET site. Therefore, the overall impact from eddy flux divergence on the upper ocean heat budget in the stratus cloud region is negligible in contrast to geostrophic and Ekman transports, which are spatially more coherent.

The results are consistent with the inspection of individual eddies in HYCOM which shows that cold waters generated near the upwelling region do not often move with eddies far west into the open ocean, including towards the IMET site. While the westward propagation of cyclonic eddies from the coast to the open ocean is often found in HYCOM, cold surface waters generated near the coast are not carried very far by these cyclonic eddies, and thus they do not significantly impact overall heat balance in the open ocean.

Our result in spatial pattern of the eddy heat flux divergence in the 50 m surface layer is similar to that in a previous observational study by Chaigneau and Pizzaro (2005a), who used Fickian law to estimate the eddy heat flux divergence, in which the World

Ocean Atlas 2001 (WOA01) temperatures are used, and the zonal and meridional components of eddy diffusivity are estimated based on the drifter trajectories. Even though using Fickian law may not be quite appropriate to describe the eddy heat flux divergence due to coherent mesoscale eddies, we did not detect a significant deviation in this case, suggesting that their results are useful here. In their study, the area averaged eddy heat flux divergence (100^{o}W-70^{o}W, 34^{o}S-10^{o}S) provides heat to the surface layer at a rate of +4.4 W m^{-2}. Such eddy flux divergence should be much smaller if averaged over the stratus region (100^{o}W-80^{o}W, 34^{o}S-10^{o}S) since the eddy flux divergence near the coast is much larger than the open ocean. The small value of eddy heat flux divergence is primarily due to its spatial incoherence.

Cold waters near the surface associated with eddies can be modified by surface heat fluxes and quickly resemble the rest of the upper mixed layer. Thus cold waters in lower portions of the eddies may be observable further from the coast as they are insulated from the atmosphere. In this case, water masses below 50 m associated with eddies could possibly influence upper ocean heat balance in the open ocean. In order to examine such a possibility, we also computed the eddy heat flux divergence in the upper 250 m from SODA and HYCOM (not shown). The results are similar to those in upper 50 m in which the eddy heat flux divergence term is not spatially coherent, although typically the magnitude at a given location is larger since it is integrated through a deeper layer.

5. Discussion

The spatial distribution of horizontal heat advection due to Ekman transport (Figure 5) indicates that it causes warming (cooling) to the north (south) of around 20^{o}S in the stratus deck region. We have also calculated the area average of each term north and south of 20°S (Table 5). Heat advection due to Ekman transport gives stronger warming in the northern part of the stratus cloud region. To the south of this region, this warming becomes much weaker in HYCOM or changes the sign in SODA. Cooling due to geostrophic transport is evident in both north and south regions, but it is weaker in the south for SODA. As indicated in the spatial distribution of the eddy heat flux divergence term, this term is negligible both north and south of 20°S. Accordingly, the contribution of each term can be very different in northern and southern parts of the stratus region, and thus additional observations such as surface buoys in locations both south and north of 20°S will help improve our understanding of upper ocean processes under the stratus cloud decks in the southeast Pacific.

There are other terms in the heat equation that are not discussed in detail. The major additional term that could significantly contribute to the heat budget is vertical diffusion (mixing). Although this term is negligible at 250 m depth (Colbo and Weller 2007), it could be comparable to other terms in the 0-50 m layer. Unfortunately, it is difficult to estimate this term accurately at 50 m from the available model output. We have also performed the same analyses in this paper for the 0-250 m layer in which the vertical diffusion term is negligible, showing that the spatial distribution of horizontal heat advection and eddy heat flux divergence terms for the 0-250 m layer are similar to those for the 0-50 m layer (not shown). However, it is possible that the vertical mixing term could contribute to the closure of the heat budget for the 0-50 m layer.

Although the analysis of HYCOM output indicates that the eddy flux divergence term is negligible in the heat budget of the entire stratus deck region in comparison to horizontal advection terms, the result could be model dependent. Also, HYCOM was integrated for only 4 years, and it is possible that the result could be different in other time periods. In fact, large interannual variations within the upper ocean associated with ENSO are evident in the stratus cloud region (Shinoda and Lin 2009). Longer integrations using multiple eddy-resolving models are necessary to further investigate the role of eddies in this region.

6. Summary

This study examines the upper ocean processes in the stratus cloud deck region using SODA data and the eddy-resolving HYCOM. The model performance is first evaluated based on comparison with *in situ* data from the IMET buoy at 85^{o}W, 20^{o}S. Then the annual mean of the upper ocean heat budget is calculated from the model output. The relative importance of physical processes responsible for the heat budget is also investigated, particularly the roles of geostrophic and Ekman transports, and the eddy heat flux. The analysis of model output was conducted for the entire stratus cloud deck region to examine the representativeness of the IMET observation site for broad scale upper ocean processes in this region.

Both SODA and HYCOM reproduce the seasonal evolution of the mixed layer reasonably well. The mean heat budget for the upper 250 m in the models is compared with the corresponding heat budget based on observations at 85^{o}W, 20^{o}S, and it demonstrates some consistencies. Net surface heat fluxes used in the HYCOM experiment provide warming in most areas of the stratus deck, including the IMET mooring site. One of the major sources of cooling that balances the positive surface heat fluxes is geostrophic transport. These results are consistent with those from observations described in Colbo and Weller (2007).

Major terms of the heat equation in the upper 50 m were also calculated over a large portion of the stratus region. The heat transport produced by mean geostrophic currents is one of the primary sources of cooling in the entire stratus region due to its spatial coherence. Although Ekman currents are generally stronger than geostrophic currents in the upper 50 m, heat transport due to geostrophic currents is comparable to that by Ekman currents. This is because the direction of geostrophic currents in this region is nearly perpendicular to the isotherms of the upper ocean temperature, while Ekman currents are nearly parallel to the isotherms. It is found that Ekman transport generates warming/cooling to the north/south of around 20^{o}S. This result is consistent with the estimates by Colbo and Weller (2007) in which Ekman heat transport is negligible at the IMET site (85^{o}W, 20^{o}S).

The role of eddies in the upper ocean heat budget is examined using the eddy-resolving HYCOM and observational data. A comparison of eddy activity in HYCOM with that derived from satellite observations (i.e., AVISO) indicates that HYCOM is capable of simulating the realistic eddies in the stratus cloud region. The results indicate that the eddy heat flux divergence term is negligible for the entire stratus region because it is not spatially coherent although it could be comparable to other terms at a particular location.

A substantial amount of data in the upper ocean and atmospheric boundary layer have been collected recently in the region of stratus cloud deck in the southeast Pacific during the VAMOS Ocean-Cloud-Atmosphere-Land Study (VOCALS) Regional Experiment

(VOCALS REx) (Wood et al. 2007). In the next few years, thorough analyses of these data sets will be conducted by many investigators. Hopefully, knowledge of the upper ocean heat budget obtained in this study will help interpret the results of their analyses.

Acknowledgments:

Data from the Stratus Ocean Reference Station were made available by Dr. Robert Weller of the Woods Hole Oceanographic Institution; these data were collected with support from Pan American Climate Study and Climate Observation Programs of Office of Global Programs, NOAA Office of Oceanic and Atmospheric Research, Grants NA17RJ1223, NA17RJ1224, and NA17RJ1225. We are thankful for the altimeter products which were produced by Ssalto/*Duacs* and distributed by *Aviso*, with support from *Cnes* (http://www.aviso.oceanobs.com/duacs/). Yangxing Zheng is supported by the NSF Grant OCE-0453046. Toshiaki Shinoda is supported by the NSF Grants OCE-0453046 and ATM-0745897, In addition, Toshiaki Shinoda, E. Joseph Metzger, and Harley Hurlburt are supported by the 6.1 project Global Remote Littoral Forcing Via Deep Water Pathways sponsored by the Office of Naval Research (ONR) under program element 601153N. Jialin Lin is supported by National Aeronautics and Space Administration (NASA) under the Modeling, Analysis, and Prediction (MAP) program and by NSF Grant ATM-0745872. Benjamin S. Giese is grateful for support from the NSF Grant OCE-0351802 and the National Oceanic and Atmospheric Administration (NOAA) Grant NA06OAR4310146.

REFERENCES

Bingham, F. M., S. D. Howden, and C. J. Koblinsky, 2002: Sea surface salinity measurements in the historical database. *J. Geophys. Res*., **107**, 8019, doi: 10.1029/2000JC000767.

Bleck, R., 2002: An oceanic general circulation model framed in Hybrid Isopycnic-Cartesian Coordinates, *Ocean Modelling*, **4**, 55-88.

Bleck, R., and S. G. Benjamin, 1993: Regional weather prediction with a model combining terrain-following and isentropic coordinates. 1. Model description. *Mon. Wea. Rev*. **121**(6), 1770-1785.

Bleck, R., and D. B. Boudra, 1981: Initial testing of a numerical ocean circulation model using a hybrid (quasi-isopycnic) vertical coordinate. *J. Phys. Oceanogr*., **11 (6)**, 755-770.

Boyer, T. P., C. Stephens, J. I. Antonov, M. E. Conkright, L. A. Locarnini, T. D. O'Brien, and H. E. Garcia, 2002: *Salinity*. Vol. 2, *World Ocean Atlas 2001*, NOAA Atlas NESDIS 49, 165 pp.

Bradley, E. F., Fairall, C. W., Hare, J. E., and Grachev, A. A.: 2000: 'An Old and Improved Bulk Algorithm for Air-Sea Fluxes', in preprint, *14th Symposium on Boundary Layer and Turbulence*, Aspen, CO, August 7–11, American Meteorological Society, 45 Beacon St., Boston, MA, pp. 294–296.

Carton, J. A., and B. S. Giese, 2008: A reanalysis of ocean climate using Simple Ocean Data Assimilation (SODA). *Mon. Wea. Rev*., **136**, 2999-3017.

Carton, J. A., G. A. Chepurin, X. Cao, and B. S. Giese, 2000a: A Simple Ocean Data Assimilation analysis of the global upper ocean 1950-1995, Part 1: methodology. *J. Phys. Oceanogr.*, **30**, 294-309.

Carton, J. A., G. A. Chepurin, and X. Cao, 2000b: A Simple Ocean Data Assimilation analysis of the global upper ocean 1950-1995, Part 2: results. *J. Phys. Oceanogr.*, **30**, 311-326.

Chaigneau, A., and O. Pizarro, 2005a: Mean surface circulation and mesoscale turbulent flow characteristicsin the eastern South Pacific from satellite tracked drifters. *J. Geophys. Res*., **110**, doi: 10.1029/2004JC002628

Chaigneau, A., and O. Pizarro, 2005b: Eddy characteristics in the eastern South Pacific. *J. Geophys. Res*., **110**, doi: 10.1029/2004JC002815.

Colbo, K, and R. Weller, 2007: The variability and heat budget of the upper ocean under the Chile-Peru stratus. *J. Mar. Res*., **65**, 607-637.

Diaz, H., C. Folland, T. Manabe, D. Parker, R. Reynolds, and S. Woodruff, 2002: Workshop on advances in the use of historical marine climate data. *WMO Bull.,* **51**, 377-380.

Gordon, C. T., A. Rosati, and R. Gudgel, 2000: Tropical sensitivity of a coupled model to specified ISCCP low clouds. *J. Climate*, **13**, 2239-2260.

Han, W., 2005: Origins and dynamics of the 90-day and 30-60day variations in the equatorial Indian Ocean. *J. Phys. Oceanogr*., **35**, 708-728.

Han, W., T. Shinoda, L-L., Fu, and J. P. McCreary, 2006: Impact of atmospheric intraseasonal oscillations on the Indian Ocean dipole. *J. Phys. Oceanogr*., **36**, 670-690.

Hormazabal, S., G. Shaffer, and O. Leth, 2004: Coastal transition zone off Chile. *J. Geophys. Res.*, **109**, C01021, doi: 10.1029/2003JC001956.

Hurlburt, H. E., E. J. Metzger, P. J. Hogan, C. E. Tilburg, and J. F. Shriver, 2008: Steering of upper ocean currents and fronts by the topographically constrained abyssal circulation. *Dyn. Atmos. Oceans*, **45**, 102-134.

Jones, P. W., 1999: First- and second-order conservative remapping schemes for grids in spherical coordinates. *Mon. Wea. Rev*., **127**, 2204-2210.

Kalnay et al., 1996: The NCEP/NCAR 40-year reanalysis project. *Bull. Amer. Meteor. Soc.*, 77, 437-470.

Kara, A. B., A. J. Wallcraft, and H. E. Hurlburt, 2005a: A new solar radiation penetration scheme for use in ocean mixed layer studies: An application to the Black Sea using a fine resolution Hybrid Coordinate Ocean Model (HYCOM). *J. Phys. Oceanogr*., **35**, 13-32.

Kara, A. B., A. J. Wallcraft, and H. E. Hurlburt, 2005b: Sea surface temperature sensitivity to water turbidity from simulations of the turbid Black Sea using HYCOM. *J. Phys. Oceanog*r., **35**, 33-54

Kara, A.B., H. E. Hurlburt, and A. J. Wallcraft, 2005c: Stability-dependent exchange coefficients for air-sea fluxes. *J. Atmos. Ocean. Technol.,* **22**(7), 1080-1094.

Klein, S. A., and D. L. Hartmann, 1993: The seasonal cycle of low stratiform clouds. *J. Climate*, **6**, 1587-1606.

Large, W. G., J. C. McWilliams, and S. C. Doney, 1994: Oceanic vertical mixing: Review and model with a nonlocal boundary layer parameterization. *Rev. Geophys*., **32**, 363-403.

Lin, J. L., 2007: The double-ITCZ problem in IPCC AR4 coupled GCMs: Ocean-atmosphere feedback analysis. *J. Climate*, **20**, 4497-4525.

Ma, C.-C., C. R. Mechoso, A. W. Robertson, and A. Arakawa, 1996: Peruvian stratus clouds and the tropical Pacific circulation: A coupled ocean-atmosphere GCM study. *J. Climate*, **9**, 1635-1645.

Mechoso, C. R., and coauthors, 1995: The seasonal cycle over the tropical Pacific in coupled ocean-atmosphere general circulation models. *Mon. Wea. Rev*., **123**, 2825-2838.

Miller, R. L., 1997: Tropical thermostats and low cloud cover. *J. Climate*, **10**, 409-440.

Penven, P., V. Echevin, J. Pasapera, F. Colas, and J. Tam, 2005: Average circulation, seasonal cycle, and mesoscale dynamics of the Peru Current System: a modeling approach. *J. Geophys. Res*., **110**, doi: 10.1029/2005JC002945.

Pizarro, O., G. Shaffer, B. Dewitte, and M. Ramos, 2002: Dynamics of seasonal and interannual variability of the Peru-Chile Undercurrent. *Geophys. Res. Lett*., **29(12)**, 1581, doi: 0.1029/2002GL014790.

Rosmond, T. E., J. Teixeira, M. Peng, T. F. Hogan, R. Pauley, 2002: Navy Operational Global Atmospheric Prediction System (NOGAPS): forcing for ocean models. *Oceanography*, **15**(1), 99-108.

Shaffer, G., O. Pizarro, L. Djurfeldt, S. Salinas, and J. Rutlant, 1997: Circulation and low frequency variability near the Chile coast: Remotely forced fluctuations during the 1991-1992 El Nino, *J. Phys. Oceanogr*., **27**, 217-235.

Shaji, C., C. Wang, G. R. Halliwell Jr., A. Wallcraft, 2005: Simulation of tropical Pacific and Atlantic Oceans using a Hybrid Coordinate Ocean Model. *Ocean Modelling*, **9**, 253-282.

Shinoda, T. and J. L. Lin, 2009: Interannual variability of the upper ocean in the southeast Pacific stratus region. *J. Climate*, in press.

Shinoda, T., P. E. Roundy, and G. E. Kiladis, 2008: Variability of intraseasonal Kelvin waves in the equatorial Pacific Ocean. *J. Phys. Oceanogr*., **38**, 921-944.

Simmons, A. J., and J. K. Gibson, 2002: The ERA-40 Projects Plan, Series #1, ECMWF, Shinfield Park, Reading, UK, 63pp.

Smith, R. D., J. K. Dukowicz, and R. C. Malone, 1992: Parallel ocean general circulation modeling. *Physica D*., **60**, 38-61.

Stephens, C. , J. I. Antonov, T. P. Boyer, M. E. Conkright, R. A. Locarnini, T. D. O'Brien, and H. E. Garcia, 2002: *Temperature*. Vol. 1, *World Ocean Atlas 2001*, NOAA Atlas NESDIS 49, 169pp.

Wood, R., C. Bretherton, B. Huebert, C. R. Mechoso, and R. Weller, 2007: The VAMOS Ocean-Cloud-Atmosphere-Land Study (VOCALS) Improving understanding, model simulations, and prediction of the Southeast Pacific Climate System. Program documents and information can be found at www.eol.ucar.edu/projects/vocals/

Xie, S.-P., 2004: The shape of continents, air-sea interaction, and the rising branch of the Hadley circulation. In the Hadley Circulation: Past, Present and Future, H. F. Diaz and R. S. Bradley (eds.), Kluwer Academic Publishers, Dordrecht.

Yu, L., and R. A. Weller, 2007: Objectively analyzed air-sea fluxes for the global ice-free oceans (1981-2005). *Bull. Amer. Meteor. Soc*., **88**, 527-539.

Yu, L., X. Jin, and R. A. Weller, 2008: Multidecade global flux datasets from the objectively analyzed air-sea fluxes (OAFlux) Project: Latent and sensible heat fluxes, ocean evaporation, and related surface meteorological variables. Woods Hole Oceanographic Institution, OAFlux Project Technical Report (OA-2008-01).

Zamudio, L., H. E. Hurlburt, E. J. Metzger, S. L. Morey, J. J. O'Brien, C. Tilburg, and J. Zavala-Hidalgo, 2006: Interannual variability of Tehuantepec eddies. *J. Geophys. Res*., **111**(C5), C05001.

Zamudio, L., H. E. Hurlburt, E. J. Metzger, and C. E. Tilburg, 2007: Tropical wave-induced oceanic eddies at Cabo Corrientes and the Maria Islands, Mexico. *J. Geophys. Res.*, **112**(C5), C05048.

Zheng, Y., and B. S. Giese, 2009: Ocean heat transport in SODA: structure and mechanisms. *J. Geophys. Res*., accepted.

FIGURE CAPTIONS

Figure 1. Time series of 5-day mean net surface heat flux (upward positive, W m^{-2}) from WHOI IMET measurements (solid line) and estimates based on NOGAPS and HYCOM's SST (dashed line) during 3 January 2004 – 8 December 2004. The zero lag correlation coefficient between the data and HYCOM in 2004 is 0.78.

Figure 2. (a) Daily mean temperature of the upper 300m at (85^{o}W, 20^{o}S) during 1 October 2004 – 31 October 2005 from WHOI IMET measurements. (b) 5-day mean temperature of the upper 300 m during the same period from SODA. (c) Same as (b) but from HYCOM. The contour interval is 1 ^{o}C.

Figure 3. Mean net surface heat flux (in W m^{-2}, downward positive) based on NOGAPS and HYCOM's SST averaged over 2003-2007. The IMET site is marked by an "X" on the map.

Figure 4. (a) Mean geostrophic heat advection (in W m^{-2}) and (c) mean geostrophic currents (in m s^{-1}), temperature (in ^{o}C) in the upper 50 m from SODA. (b) and (d) are the same as (a) and (c) but from HYCOM. The periods for the averaging are January 1980-November 2005 for SODA, and January 2003-April 2007 for HYCOM. The color bar below the bottom left (right) panel is for geostrophic heat advection (temperature).

Figure 5. The same as Figure 4 but for non-geostrophic transport (primarily Ekman transport) in the upper 50 m. The Ekman currents are approximated as the residual of total currents minus the geostrophic currents in this figure. The color bar below the bottom left (right) panel is for Ekman heat advection (temperature).

Figure 6. The mean advective heat flux in the mixed layer due to Ekman transport (filled contours in W m^{-2}), mixed layer temperature (green contours in ^{o}C), and Ekman transport using ERA-40 wind stress (1980-2001) and QuikSCAT wind stress (2002-2005) (arrows in m^2 s^{-1}) (From SODA)

Figure 7. (a) Vertical heat advection (in W m^{-2}) in the upper 50 m and (b) its ocean circulation (velocity vectors in m s^{-1}) and temperature (filled contour in ^{o}C) in the zonal-vertical plane at $20^{o}S$ averaged over 1980-2005 from SODA. The strong upwelling near the coast gives rise to cold vertical heat advection. Downward flow almost parallel to isotherm causes relatively weak warm vertical heat advection in the entire cloud deck region.

Figure 8. Maps of eddy activity represented by the temporal mean of surface eddy kinetic energy derived from geostrophic velocity for (a) SODA, (b) HYCOM, and (c) AVISO. The periods for averages are 1980-2005 for SODA, 2003-2007 for HYCOM, and 22 August 2001-28 February 2009 for AVISO. The primed terms are deviations from seasonally averaged values. Unit: cm^2 s^{-2}

Figure 9. The same as Figure 8 except that the eddy kinetic energy is computed using the total velocity for (a) SODA and (b) HYCOM. (c) AVISO remains the same as in Figure 8c.

Figure 10. Ocean states at 30 m in HYCOM on two dates. (a) Temperature (shading contours in ^{o}C) and Currents (vectors in m s^{-1}), and (b) relative vorticity (in 10^{-6} s^{-1}), and (c) Okubo-Weiss Parameter (in 10^{-12} s^{-2}) on January 8 2004. (d), (e), and (f) are the same as (a), (b), and (c) except on June 21 2004. The color bars on right upper, middle, and lower panels are for temperature, vorticity, and Okubo-Weiss Parameter, respectively.

Figure 11. Maps of temperature anomalies (filled contours in ^{o}C) along with velocity anomaly vectors (arrows in m s^{-1}) averaged in the upper 50 m during March 2005 are illustrated for the evolution of cyclonic eddies (i.e., cold eddy) in HYCOM. The offshore propagation of a cold eddy is marked by green ellipses. Anomalies of temperature and velocity are derived from the 2003-2007 pentad climatology.

Figure 12. Maps of mean eddy heat flux divergence in the upper 50 m for (a) SODA and (b) HYCOM. (Unit: W m^{-2}).

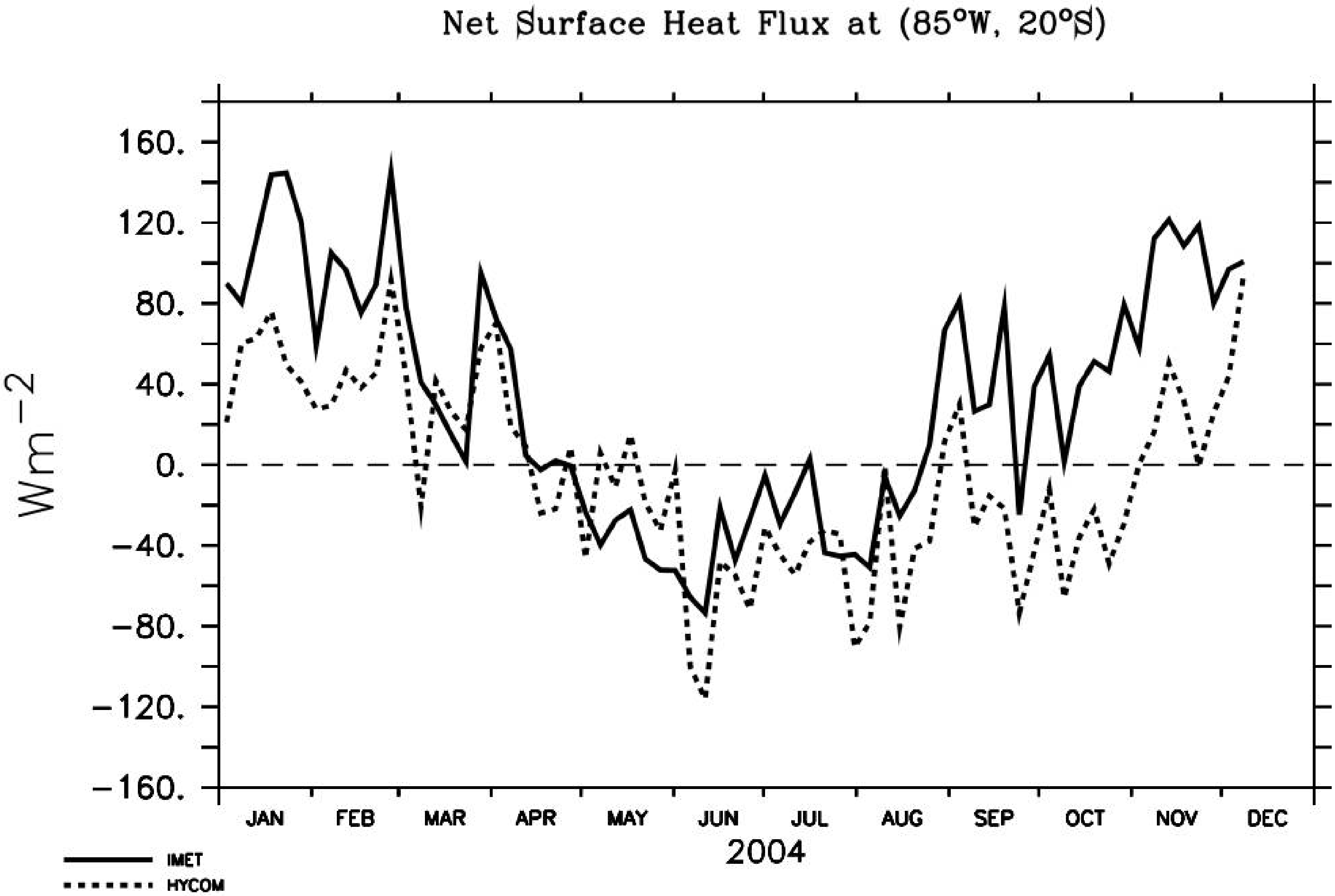

Figure 1. Time series of 5-day mean net surface heat flux (upward positive, W m^{-2}) from WHOI IMET measurements (solid line) and estimates based on NOGAPS and HYCOM's SST (dashed line) during 3 January 2004 - 8 December 2004. The zero lag correlation coefficient between the data and HYCOM in 2004 is 0.78.

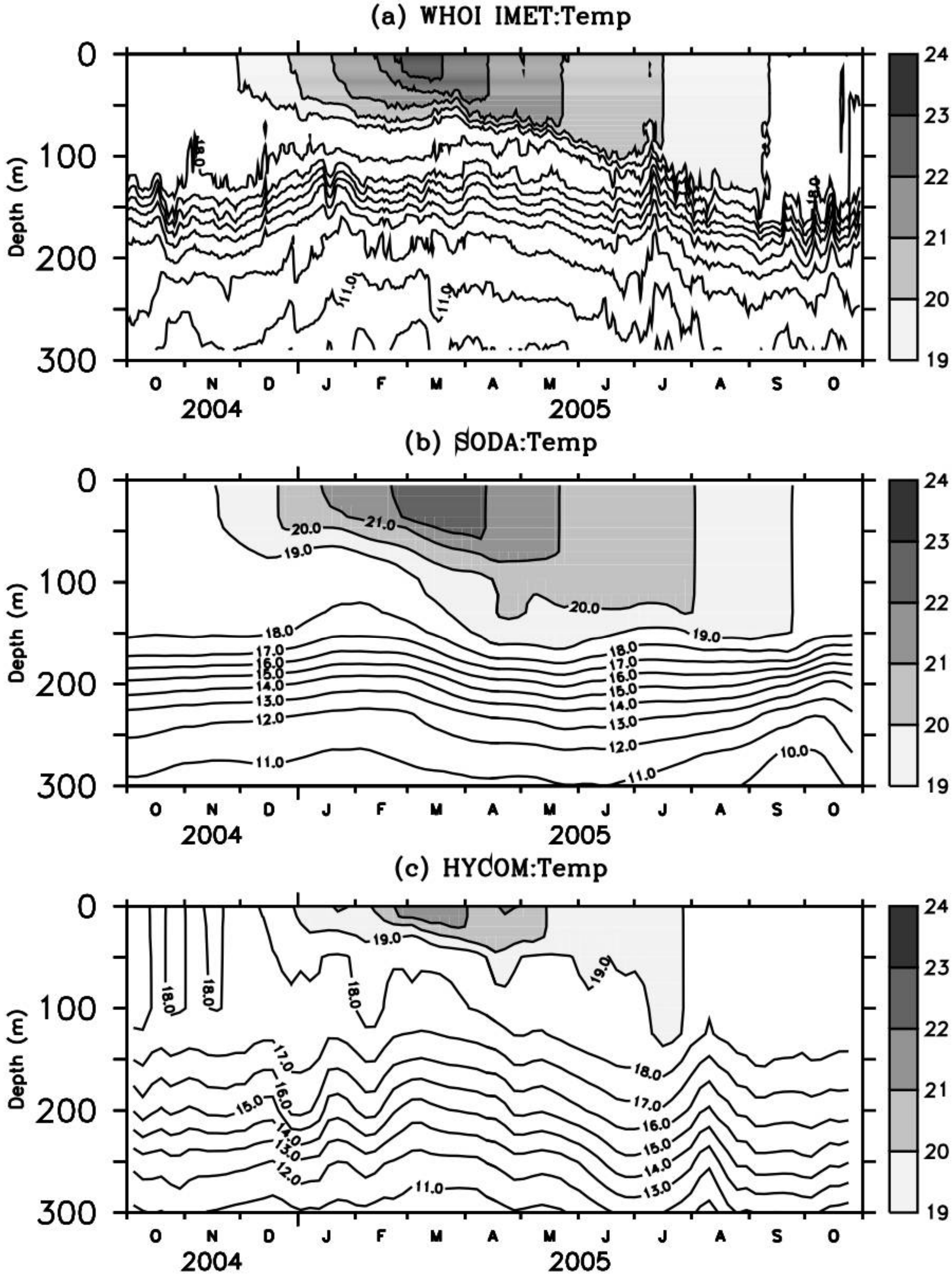

Figure 2. (a) Daily mean temperature of the upper 300 m at (85^{o}W, 20^{o}S) during 1 October 2004 - 31 October 2005 from WHOI IMET measurements. (b) 5-day mean temperature of the upper 300 m during the same period from SODA. (c) Same as (b) but from HYCOM. The contour interval is 1 ^{o}C.

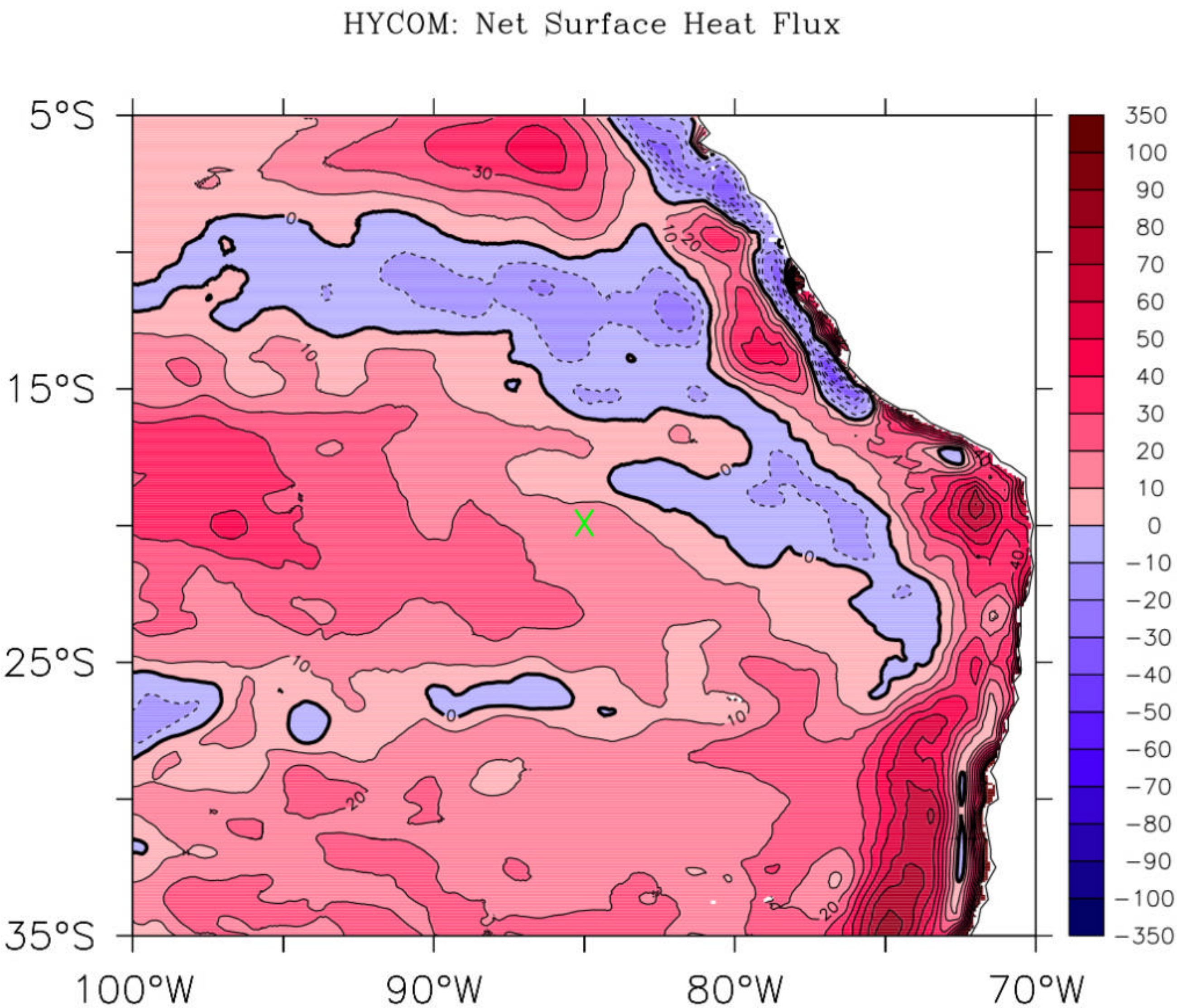

Figure 3. Mean net surface heat flux (in W m^{-2}, downward positive) based on NOGAPS and HYCOM's SST averaged over 2003-2007. The IMET site is marked by an "X" on the map.

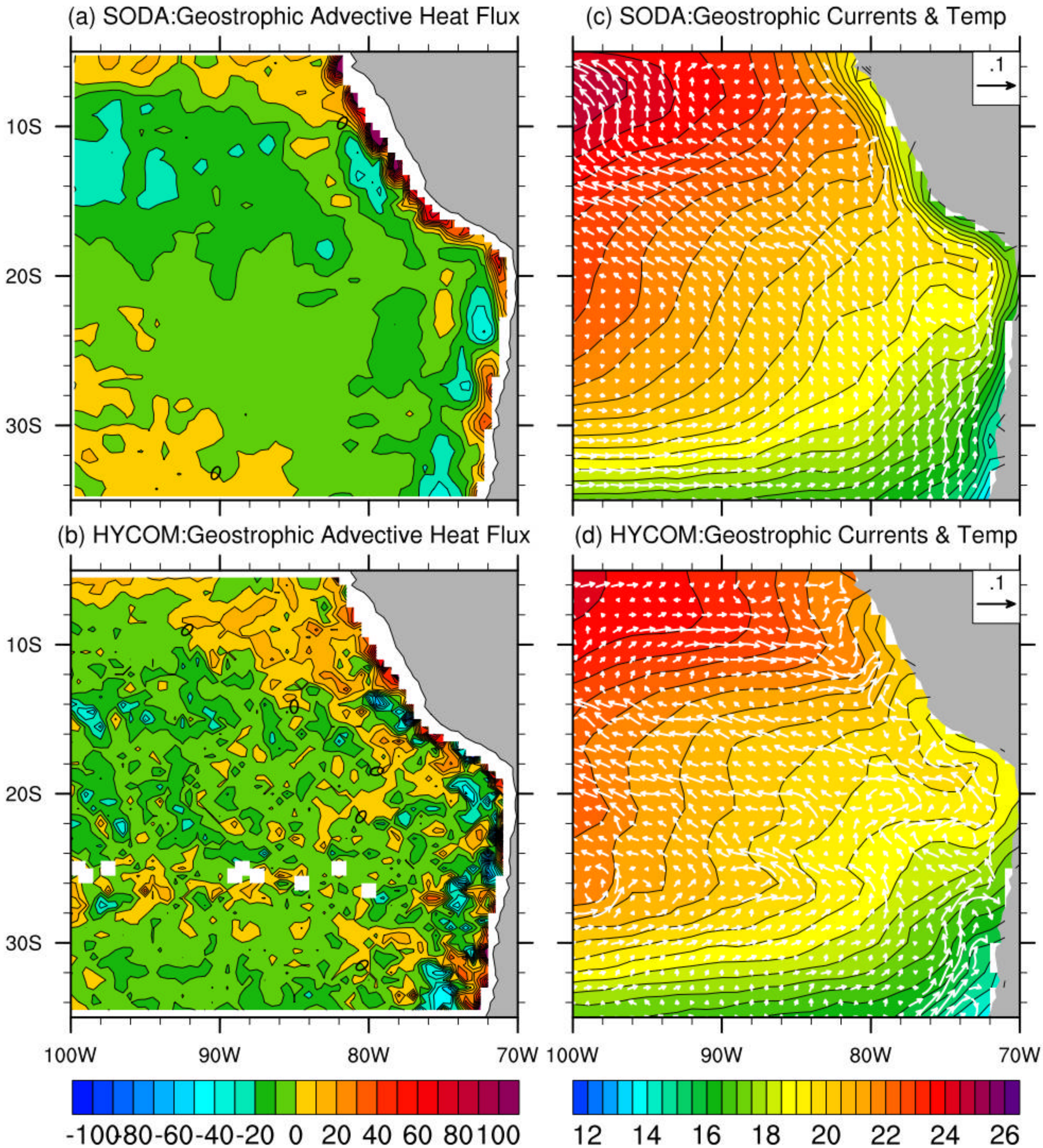

Figure 4. (a) Mean geostrophic heat advection (in W m^{-2}) and (c) mean geostrophic currents (in m s^{-1}), temperature (in ^{o}C) in the upper 50 m for SODA, (b) and (d) are the same as (a) and (c) but from HYCOM. The periods for the averaging are 1980-2005 for SODA, and 2003-2007 for HYCOM. The color bar below the bottom left (right) panel is for geostrophic heat advection (temperature).

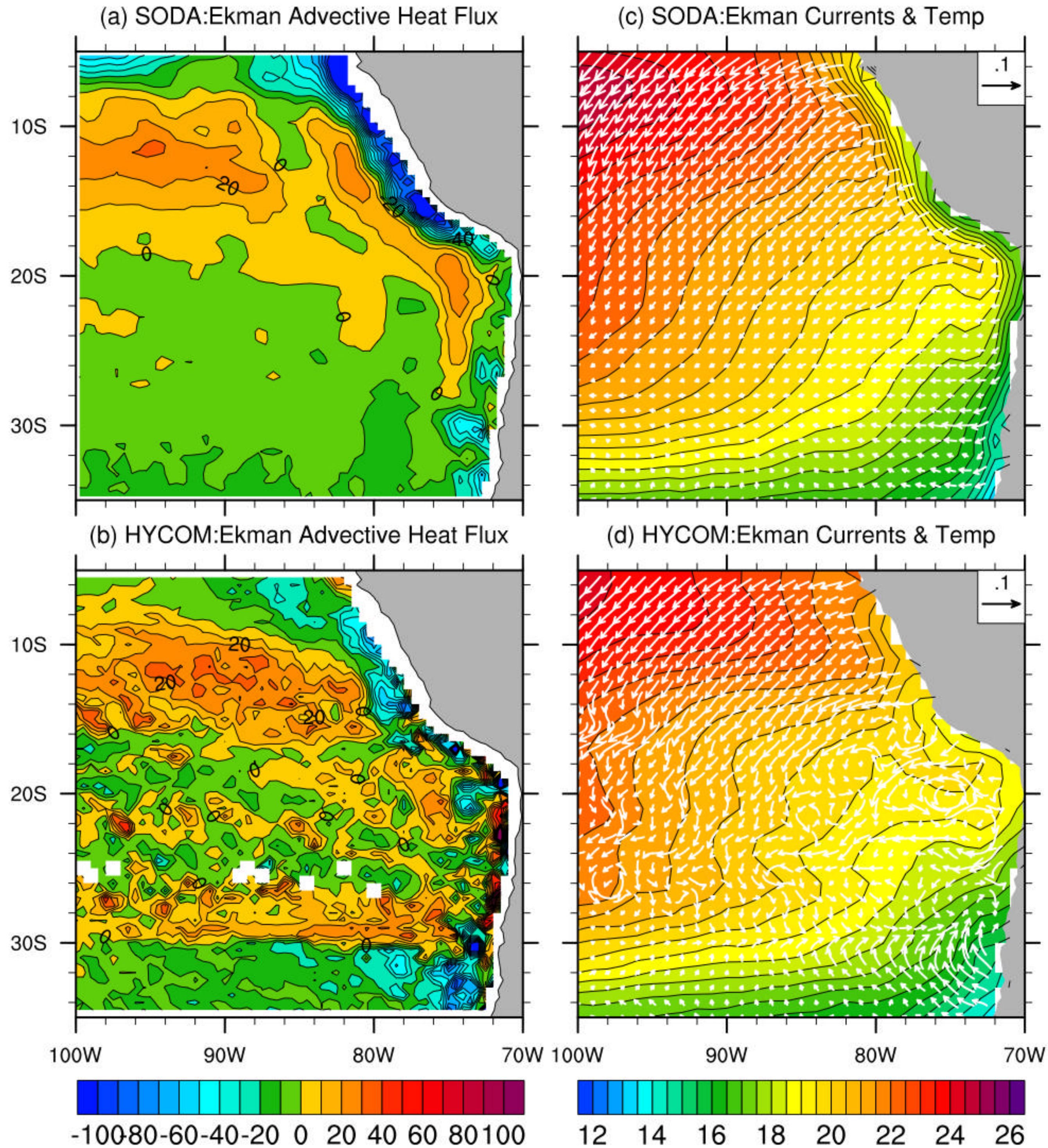

Figure 5. The same as Figure 4 but for non-geostrophic transport (primarily Ekman transport) in the upper 50 m. The Ekman currents are approximated as the residual of total currents minus the geostrophic currents in this figure. The color bar below the bottom left (right) panel is for Ekman heat advection (temperature).

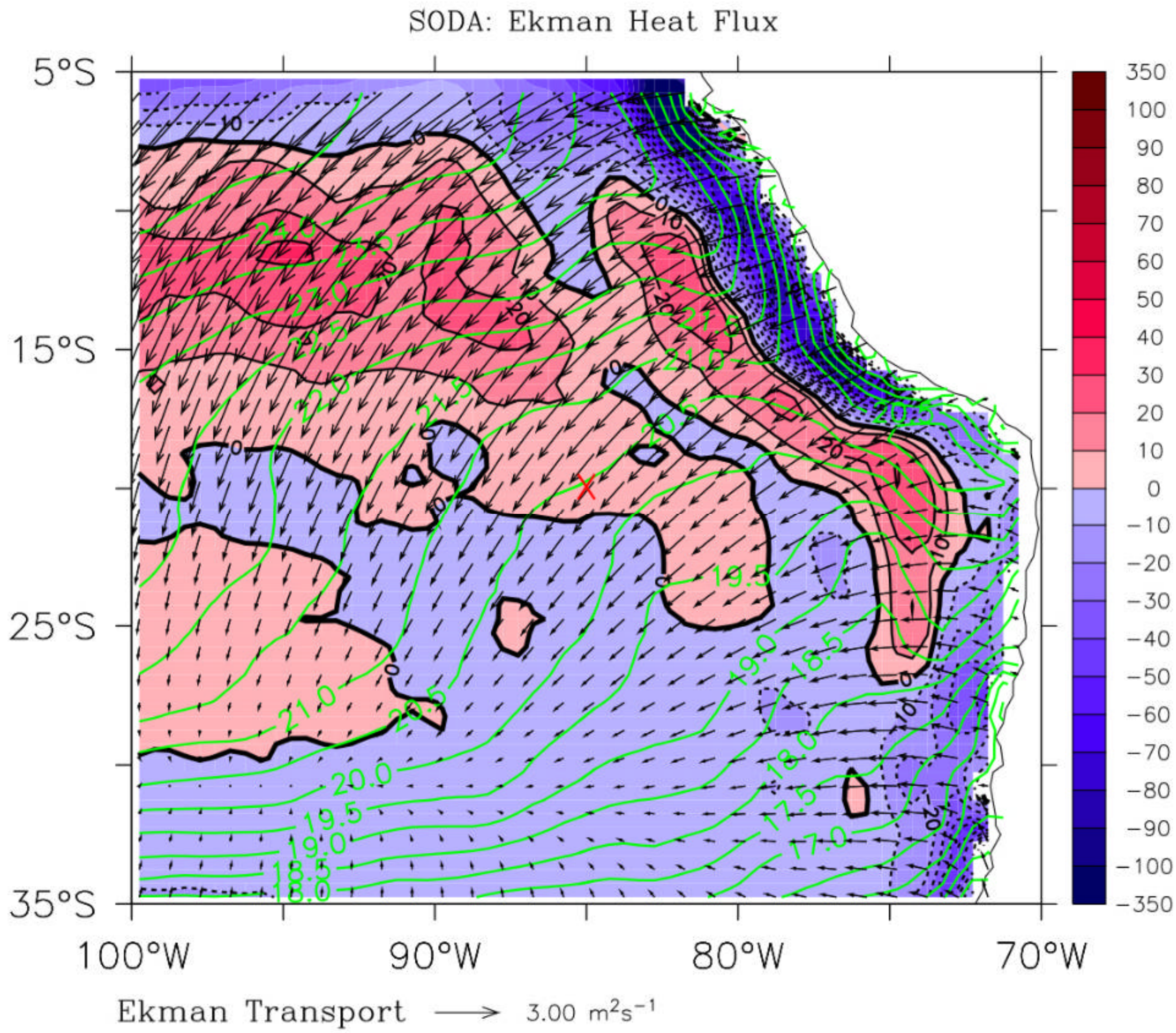

Figure 6. The mean advective heat flux in the mixed layer due to Ekman transport (filled contours in W m^{-2}), mixed layer temperature (green contours in ^{o}C), and Ekman transport using ERA-40 wind stress (1980-2001) and QuikSCAT wind stress (2002-2005) (arrows in m^{2} s^{-1}) (From SODA)

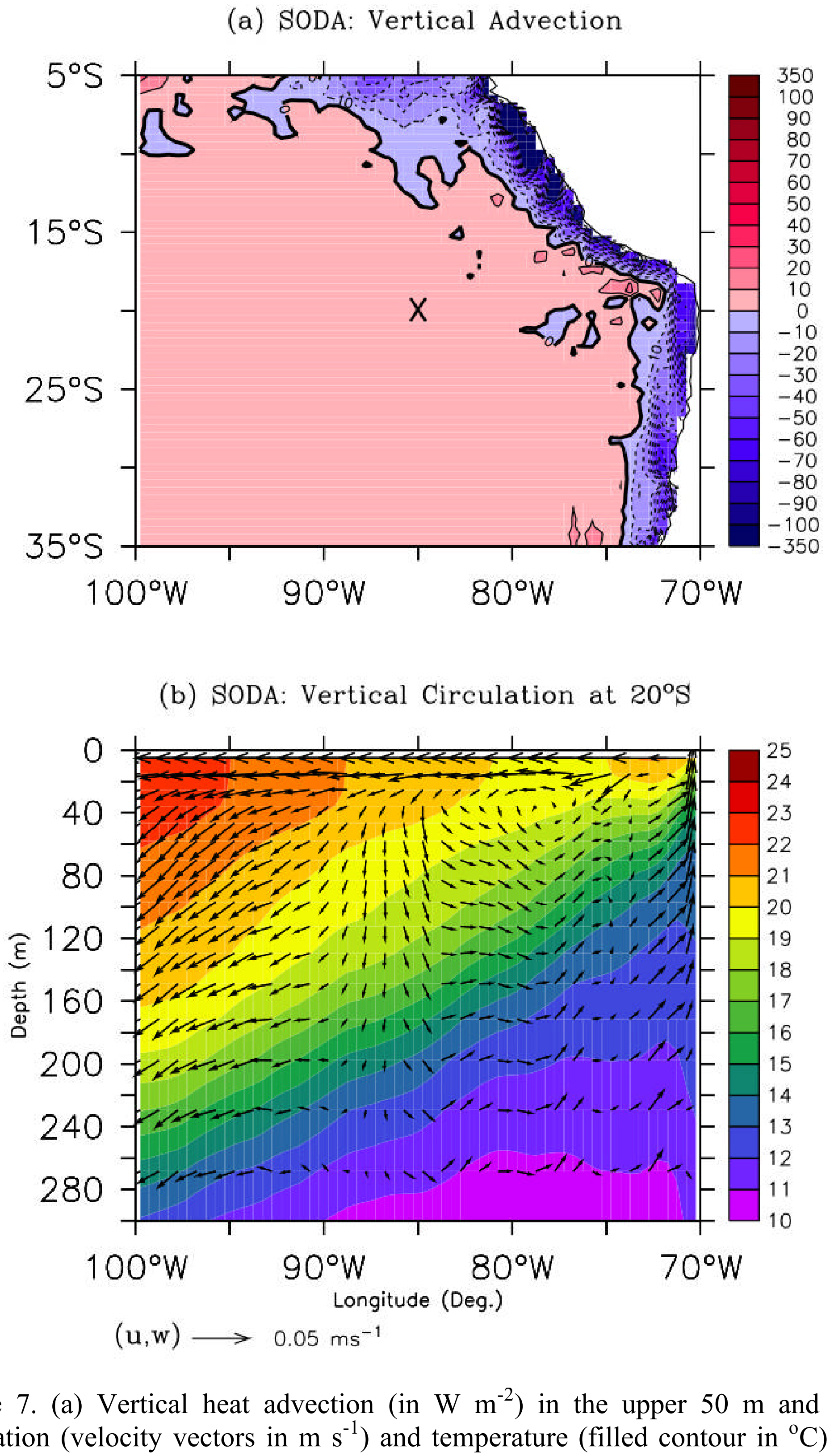

Figure 7. (a) Vertical heat advection (in W m^{-2}) in the upper 50 m and (b) its ocean circulation (velocity vectors in m s^{-1}) and temperature (filled contour in ^{o}C) in the zonal-vertical plane at 20^{o}S averaged over 1980-2005 from SODA. The strong upwelling near the coast gives rise to cold vertical heat advection. Downward flow almost parallel to isotherm causes relatively weak warm vertical heat advection in the entire cloud deck region.

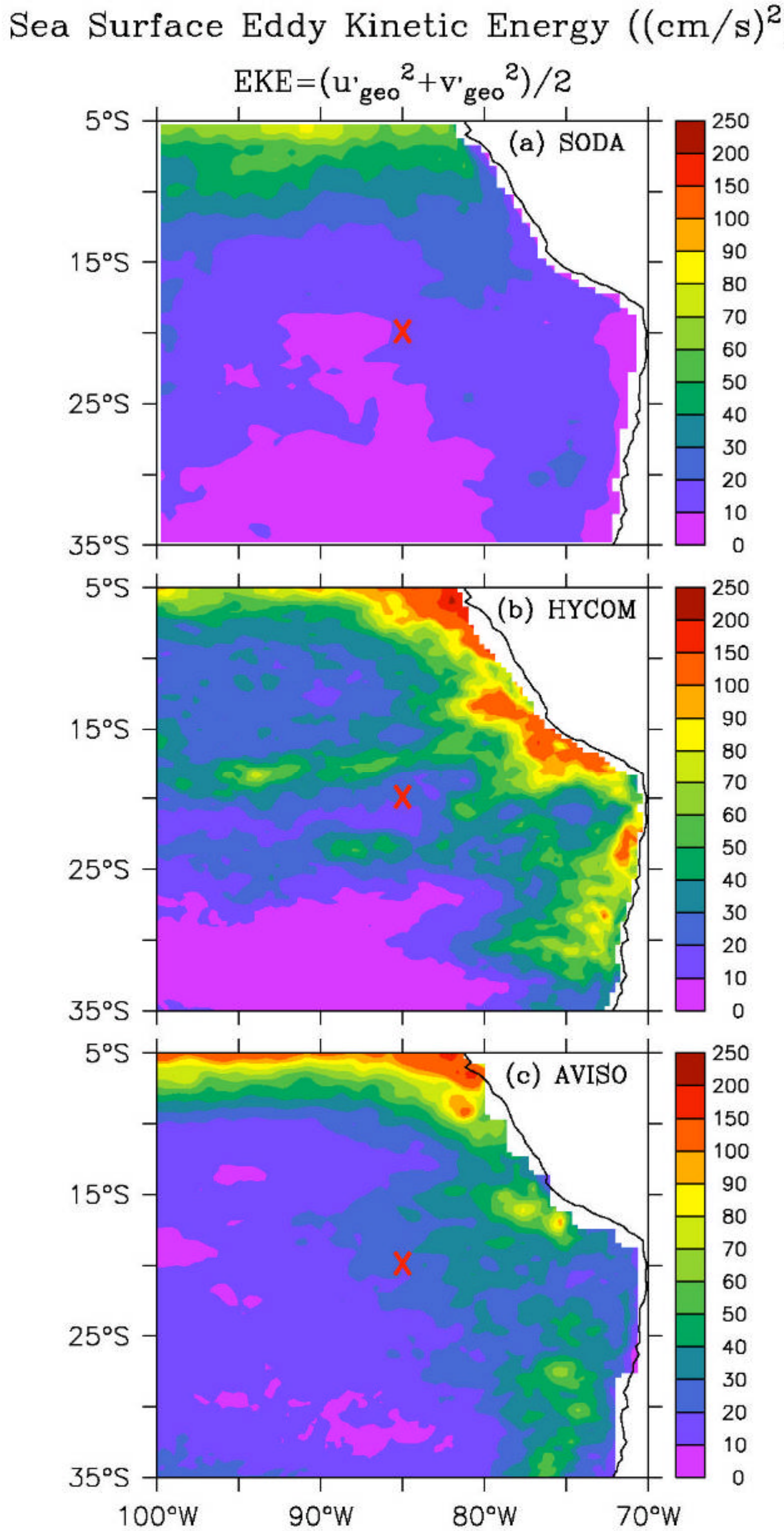

Figure 8. Maps of eddy activity represented by the temporal mean of surface eddy kinetic energy derived from geostrophic velocity for (a) SODA, (b) HYCOM, and (c) AVISO. The periods for averages are 1980-2005 for SODA, 2003-2007 for HYCOM, and 22 August 2001-28 February 2009 for AVISO. The primed terms are deviations from seasonally averaged values. Unit: cm^2 s^{-2}

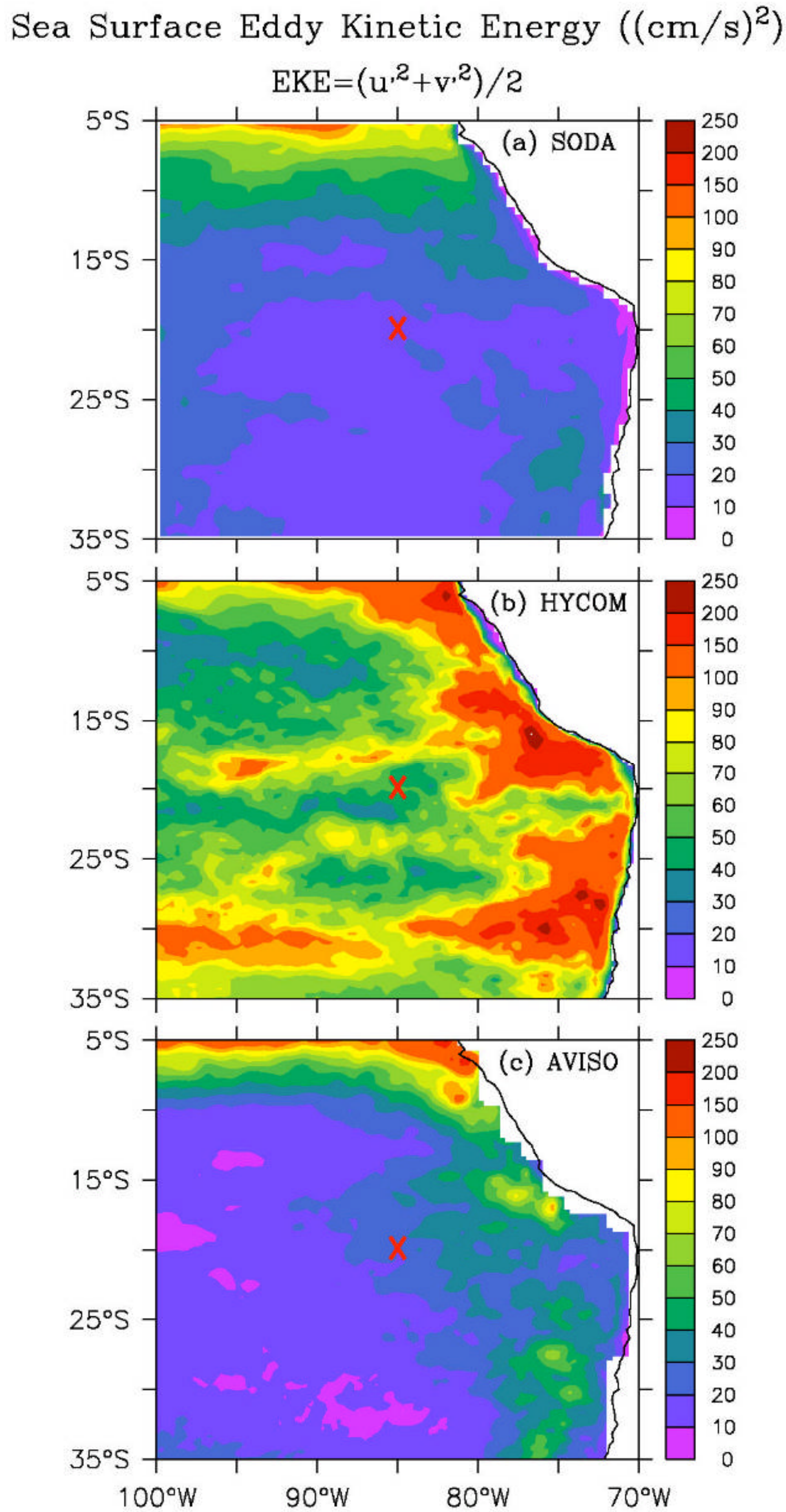

Figure 9. The same as Figure 8 except that the eddy kinetic energy is computed using the total velocity for (a) SODA and (b) HYCOM. (c) AVISO remains the same as in Figure 8c.

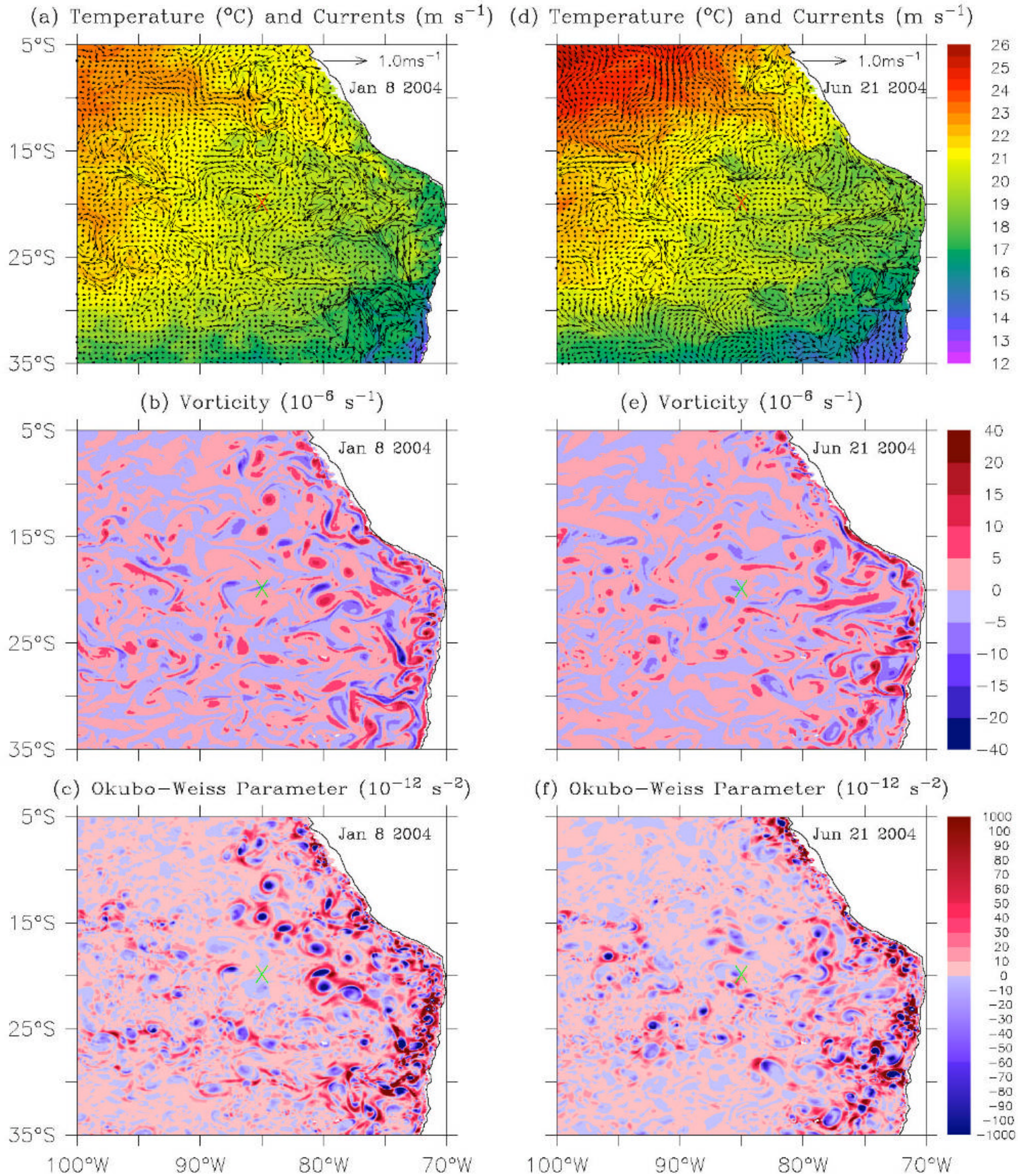

Figure 10. Ocean states at 30 m in HYCOM on two dates. (a) Temperature (shading contours in ^{o}C) and Currents (vectors in m s^{-1}), and (b) relative vorticity (in 10^{-6} s^{-1}), and (c) Okubo-Weiss Parameter (in 10^{-12} s^{-2}) on January 8 2004. (d), (e), and (f) are the same as (a), (b), and (c) except on June 21 2004. The color bars on right upper, middle, and lower panels are for temperature, vorticity, and Okubo-Weiss Parameter, respectively.

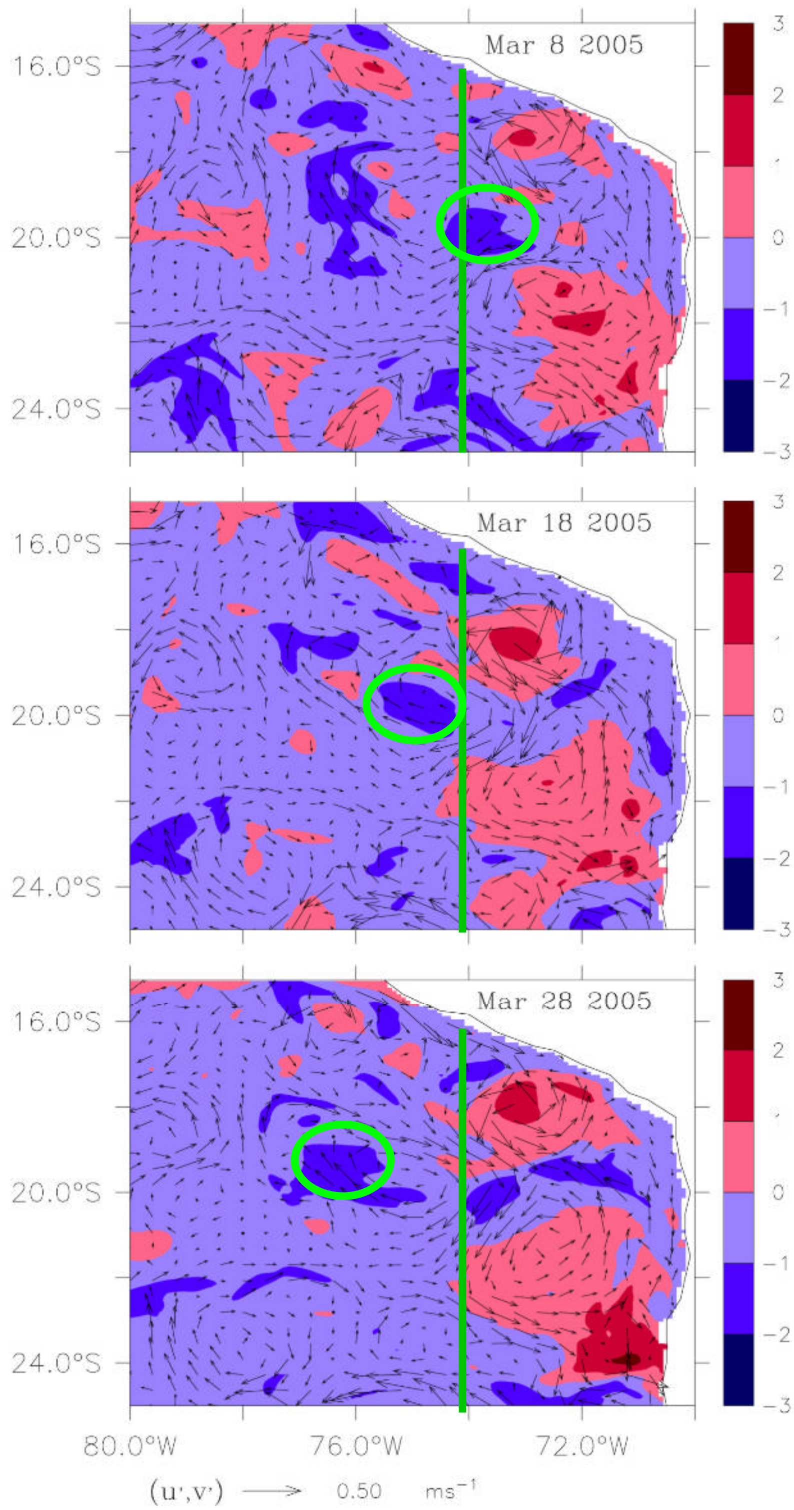

Figure 11. Maps of temperature anomalies (filled contours in ^{o}C) along with velocity anomaly vectors (arrows in m s^{-1}) averaged in the upper 50 m during March 2005 are illustrated for the evolution of cyclonic eddies (i.e., cold eddy) in HYCOM. The offshore propagation of a cold eddy is marked by green ellipses. Anomalies of temperature and velocity are derived from the 2003-2007 pentad climatology.

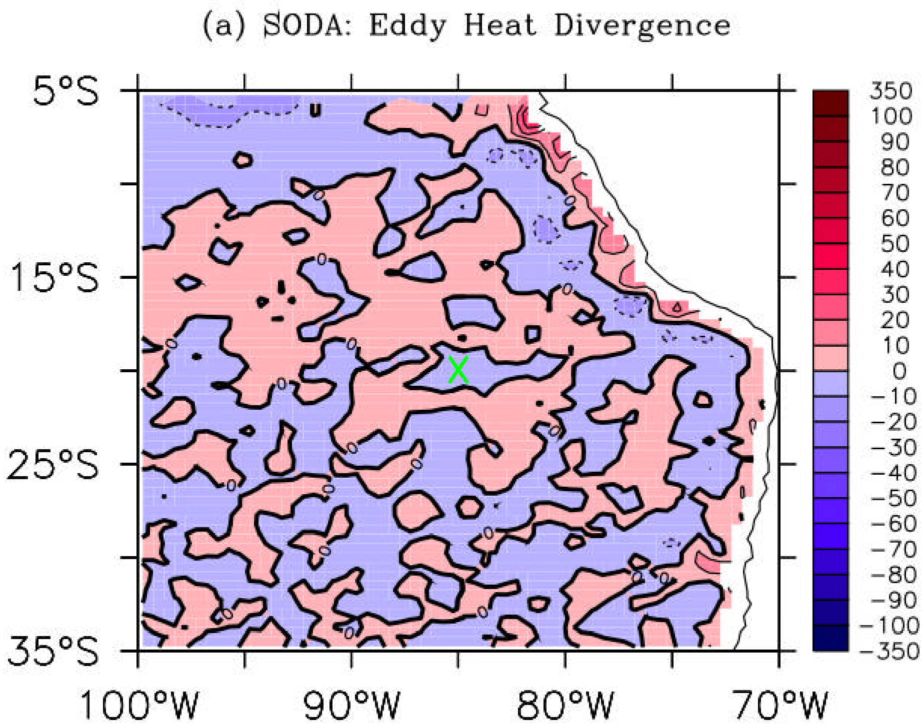

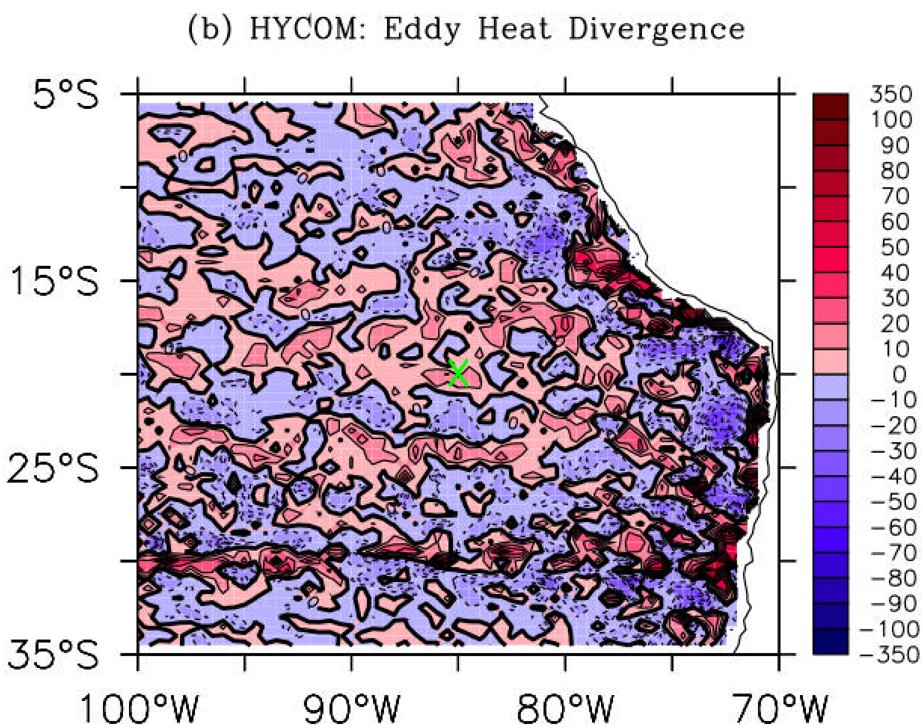

Figure 12. Maps of mean eddy heat flux divergence in the upper 50 m for (a) SODA and (b) HYCOM. (Unit: W m^{-2}).

Table 1. Comparison between Colbo and Weller's estimates based on the IMET buoy datasets (0-250 m) and the models (0-250 m) in the upper ocean heat budget. The periods for the averaging are October 2000 to December 2004 for Colbo and Weller's (2007) estimates, January 1980 to November 2005 for SODA, and January 2003 to April 2007 for HYCOM (Unit: W m^{-2})

(85°W, 20°S)	Q_{net}	$-\mathbf{V}_{geo} \bullet \nabla T$	$-\mathbf{V}_{ek} \bullet \nabla T$	$-\nabla \cdot \left(\overline{\mathbf{V}'T'}\right)$
Colbo & Weller (2007)	44	-20	6	-30
SODA		-21	11	-19
HYCOM	18	-45	-44	42

Table 2. Ocean heat budget (0-250 m) averaged over the region (100^{o}W-80^{o}W, 30^{o}S-10^{o}S) from SODA and HYCOM. The periods for the averaging are January 1980 to November 2005 for SODA, and January 2003 to April 2007 for HYCOM (Unit: W m^{-2})

100^{o}W-80^{o}W, 30 ^{o}S-10 ^{o}S	Q_{net}	$-\mathbf{V}_{geo} \bullet \nabla T$	$-\mathbf{V}_{ek} \bullet \nabla T$	$-\nabla \cdot \left(\overline{\mathbf{V}'T'}\right)$
SODA		-27	0.1	-0.4
HYCOM	11	-23	7	-1

Table 3. Ocean heat budget in the upper 50 m at the IMET site from SODA and HYCOM. The periods for the averaging are the same as in Table 2 (Unit: W m^{-2})

(85^{o}W, 20^{o}S)	Q_{net}	$-\mathbf{V}_{geo} \bullet \nabla T$	$-\mathbf{V}_{ek} \bullet \nabla T$	$-\nabla \cdot \left(\overline{\mathbf{V}'T'}\right)$
SODA		-6	4	-3
HYCOM	18	-10	-8	6

Table 4. Ocean heat budget in the upper 50 m averaged over the region (100°W-80°W, 30°S-10°S) from SODA and HYCOM. The periods for the averaging are the same as in Table 2 (Unit: W m^{-2})

100°W-80°W, 30°S-10°S	Q_{net}	$-\mathbf{V}_{geo} \bullet \nabla T$	$-\mathbf{V}_{ek} \bullet \nabla T$	$-\nabla \cdot \left(\overline{\mathbf{V}'T'}\right)$
SODA		-9	3	0.1
HYCOM	11	-5	6	-0.1

Table 5. Ocean heat budget in the upper 50 m averaged over the region (100°W-80°W, 20°S-10°S) and (100°W-80°W, 30°S-20°S) from SODA and HYCOM. The periods for the averaging are the same as in Table 2 (Unit: W m^{-2})

100°W-80°W, 20°S-10°S	Q_{net}	$-\mathbf{V}_{geo} \bullet \nabla T$	$-\mathbf{V}_{ek} \bullet \nabla T$	$-\nabla \cdot \left(\overline{\mathbf{V}'T'}\right)$
SODA		-13	9	0.4
HYCOM	7	-6	10	-0.2
100°W-80°W, 30°S-20°S				
SODA		-4	-3	-0.2
HYCOM	14	-5	2	0.1